Anticancer Potential of Dendritic Poly(aryl ether) Substituted Polypyridyl Ligands Based Ruthenium(II)-Coordination entities

Liju Raju[a], Sousa Javan Nikkhah[b], MosaChristas K[c] , Matthias Vandichel[b], and Eswaran Rajkumar[a*]

[a] Department of Chemistry, Madras Christian College (Autonomous), Affiliated to the University of Madras, Tambaram East, Chennai, Tamilnadu, India 600059.

[b] Department of Chemical Sciences and Bernal Institute, University of Limerick,Limerick V94 T9PX, Republic of Ireland

[c] Department of Plant Biology and Biotechnology & Loyola Institute of Frontier Energy (LIFE), Loyola College (Autonomous), University of Madras, Chennai, India 600034

Email: rajjkumar@gmail.com

Abstract

This paper studies the anticancer potency of dendritic poly(aryl ether) substituted polypyridyl ligands based Ruthenium(II)- coordination entities. The dendritic coordination entities were successfully designed, synthesized, and characterized by different spectral methods such as Fourier transform infrared (FT-IR), ^{1}H and ^{13}C NMR, and mass spectrometry. Further, to understand the structure and solvation behaviour of the coordination entities, we performed all-atom molecular dynamics (MD) simulations. The behaviour, configuration, and size of the coordination entities in DMSO and water were studied by calculating the radius of gyration (R_g), and solvent-accessible surface area (SASA). The MTT assay was used to assess the *in vitro* cytotoxicity of all the coordination entities against cancerous A549 (lung cancer cells), MDA MB 231 (breast cancer cells), and HepG2 (liver cancer cells) and was found to be good with comparable IC_{50} values with respect to the standard drug cisplatin. The coordination entities exhibited dose-dependent, the highest activity was shown against HepG2 cell lines in comparison to the other cancer cell lines. In addition, fluorescence staining studies, such as AO/EB, DAPI, and cell death analysis by PI staining, were performed on the coordination entities to understand the apoptosis mechanism. Furthermore, reactive oxygen species (ROS) and mitochondrial membrane potential (MMP) assays confirm apoptosis in cancer cells via the mitochondrial pathway. The DNA fragmentation assay was done followed by Molecular docking analysis with DNA was executed to strengthen and support the experimental observations.

Keywords: Dendritic poly(aryl ether) complexes, coordination entities, anticancer, *in vitro* cytotoxicity, molecular dynamic simulations, molecular docking

1. Introduction

Ruthenium(II) coordination entities or commonly known as ruthenium(II) complexes have showcased remarkable potential as anticancer drugs compared to other platinum-based analogues; however, their poor drug delivery efficiency is a major challenge which curtails their limitless application in cancer treatment[1–3]. The emergence of nanomaterials has paved the way for a new dimension of advanced cancer therapy; anticancer drugs bound to nanoparticles are known to exhibit highly efficient targeted drug delivery[4–6]. The typical drug transport mechanisms of metallodrugs have been passive diffusion, active transport, and endocytosis[7,8]. However, for nanoparticle-based metallodrugs there are new transport and cellular uptake routes because of the phenomenon known as enhanced permeability and retention effect (EPR effect)[9–13]. This effect has been extensively exploited in cancer therapies and has shown promising results. The nanoparticles-conjugated anticancer drugs have been widely developed with targeted drug delivery, avoiding healthy cells and minimal side effects.

During the last decades' several nanomaterials conjugated ruthenium complexes have been developed exhibiting enhanced anticancer activity, e.g. ruthenium-conjugated gold[14], selenium[15,16], silicon nanoparticles[17], ruthenium-carbon nanoparticles[18], and dendrimers-based ruthenium complexes. Among several nanoscopic delivery systems, dendrimers have become more attractive for drug delivery applications.

The ruthenium complexes combined with dendritic nanostructures have been developed for enhanced cancer therapies; the most studied Ru(II) based dendrimers are those of carbosilanes which have shown activity against leukaemia, prostate ,cervical, breast, colorectal kidney and lung cancer cell lines[19–24]. Govender et al. reported poly(propylene imine) type of dendrimers used in combination with Ru(II) complexes showing cytotoxicity[25]. These poly(propylene imine) dendrimeric Ru(II) complexes have shown higher anticancer activity against ovarian carcinoma[26,27]. However, most Ruthenium based metallodendrimers exhibiting anticancer properties have been found to be multinuclear systems with more than one metal centre; this may induce metal toxicity[28], thus incorporating minimal metal centres with efficient targeted metallodendrimers would be viable solution. Thus the two challenges; poor drug delivery and multinuclear metallic systems induced metal toxicity can be overcome by the development Ru(II) cored amphiphilic dendrimeric systems, which renders them extremely promising for cancer therapeutics.

In recent times, researchers have been focusing on the use of amphiphilic dendrimers to enhance the biological activities such as imaging, drug delivery, and sensors etc[29,30]. The development of amphiphilic structures solely depends on the architectural design of the

molecules. Typically, an amphiphilic system comprises of three different units: the surface group, the interior branches, and the core. The amphiphilicity can be brought in by carefully choosing the surface groups, for example, poly(ethylene glycol) (PEG) has been widely used as a surface group on dendrons for inducing amphiphilicity[29,31]. On the other hand, the surface group can also account for the lipophilicity, membrane permeability, solubility, toxicity, structural stability, responses to external stimuli and selectivity when it comes to site targeted applications[32], hence, a careful selection of the surface end groups is very significant. Anionic and neutral dendrimers are found to be biocompatible, while the cationic dendrimers have exhibited generation dependency degrees of cytotoxicity. The surface charge also plays a key role in dendrimer-membrane interactions, the surface charges on dendrimers are found to significantly disrupts the membrane integrity[33], which is often accepted as a mechanism of cytotoxicity induced by dendrimers. For example, ester groups at the surfaces can easily induce amphiphilicity and they are known to be less toxic[34]. The inner dendritic branches are the backbone of the system, compared to other types of dendrimers such as PAMAM,[35,36] the poly(aryl ether) dendrimers can be easily synthesized and customized at their core and periphery. Further, the poly(aryl ether) are known to be engaged in photonic studies and applications like sensors[37], and light harvesting applications[38–43]. Recently poly(aryl ether) based amphiphilic dendrons were constructed for drug delivery, anticancer, and antibacterial applications[44–47]. Finally, a suitable core group is chosen to act as chelating ligand, which could coordinate with Ru(II) ions to form metallodendrimers for various anticancer applications.

Based on the above hypothesis, in our previous work[32], we have reported the design and synthesize of novel *tert*-butyl ester functionalized dendritic poly(aryl ether) bipyridyl amphiphilic ligands, which can be readily complexed with Ru(II) ions. Thus, in this work, we focus on synthesizing *tert*-butyl ester functionalized dendritic poly(aryl ether) based Ru(II) polypyridyl coordination entities and evaluating their *in vitro* anticancer potency.

2. Experimental

2.1. Materials

The synthesis of poly(aryl ether) dendrons, G0-OH, G1-OH and G2-OH were carried out by following the reported literature with some appropriate modifications.[48] The detailed experimental procedure and the characterizations of ligands (see **Figure 1**) are given in our previous report.[32]

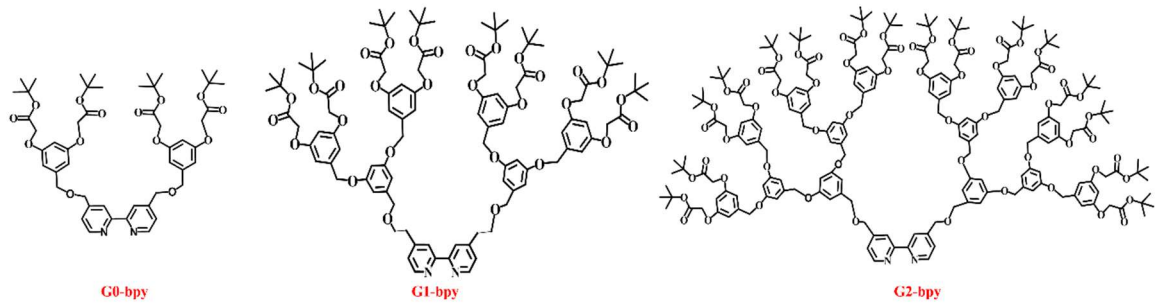

Figure 1 The synthesized poly(aryl ether) dendritic ligands

2.2. Synthesis of Ruthenium (II)-cored metallodendrons

Synthesis of [Ru(bpy)$_2$Gn-bpy]Cl$_2$ coordination entities

A mixture of [Ru(bpy)$_2$Cl$_2$].xH$_2$O[49] and corresponding Gn-bpy (n=0-2) ligands was refluxed in ethanol under inert atmosphere. The solvent was removed under vacuum, and the obtained residue was dissolved in dichloromethane and washed three times with water. The organic layer was separated, and the solvent evaporated under vacuum. The obtained residue was purified by silica column chromatography, using dichloromethane/methanol mixtures as eluant, to obtain the [Ru(bpy)$_2$G0-bpy]Cl$_2$ **(RuG0)**, [Ru(bpy)$_2$G1-bpy]Cl$_2$ **(RuG1)** and [Ru(bpy)$_2$G2-bpy]Cl$_2$ **(RuG2)** (see **Figure 2**). All the FTIR, ^{1}H-NMR, ^{13}C-NMR, and mass spectra of the synthesized Ru(II) coordination entities are provided in **Figures S1 – S12.**

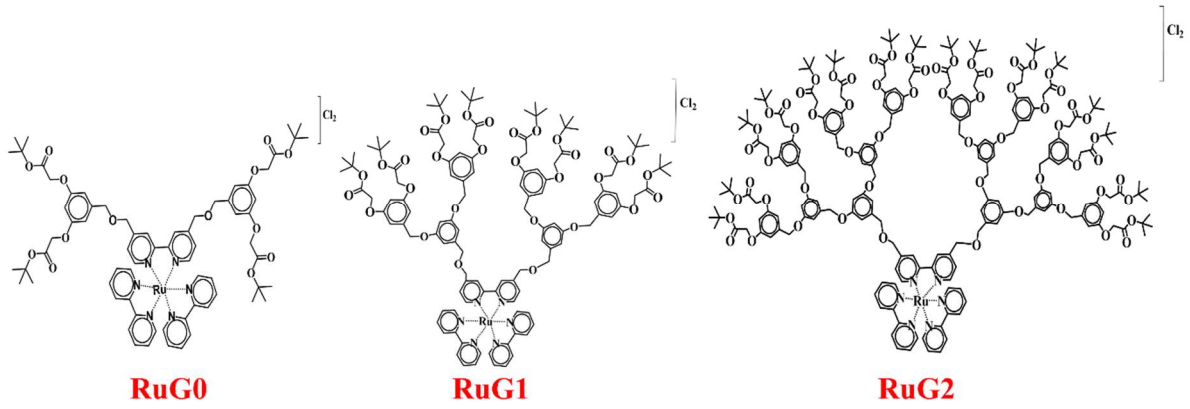

Figure 2 The synthesized [Ru(bpy)$_2$Gn-bpy]Cl$_2$ coordination entities

2.3. Instrumentations

^{1}H-NMR spectra were recorded on a Bruker 400 MHz and 500 MHz spectrometer in acetone d$_6$ solvent, ^{13}C-NMR was recorded on 100 MHz Bruker spectrometer in acetone d$_6$. ESI MS was recorded using XEVO-G2 XS QTOF (Waters Corporation, Milford, MA) mass

spectrometer in positive mode. FTIR spectra was recorded on SHIMADZU, IRTRACER 100, Japan. The fluorescence images for the anticancer activities were viewed using Invitrogen EVOS FL Cell Imaging, Thermo Fisher. The synthesized Ru(II) coordination entities were water insoluble, due to the presence of the strong hydrophobic *tert*-butyl group, hence for all biological applications the coordination entities were prepared as solutions in molecular biology grade DMSO.

2.4 Molecular simulation Studies

All simulations were performed using LAMMPS (29th September 2021)[50] (https://www.lammps.org) for the molecular dynamics (MD) simulations. VMD 1.9.3[51] (http://www.ks.uiuc.edu/Research/vmd/) was used for visualization and post-processing. A cut-off of 12 Å was applied for short-range non-bonded interactions. The Ewald summation[52] method was used to calculate long-range electrostatic interactions. To integrate Newton's equations of motion, the Verlet velocity scheme was utilized with a time step of 1 fs. For all cases, periodic boundary conditions were implemented using cubic boxes. All other details of the computational molecular simulation studies are provided in the Supporting Information (Section 2.1-2.2).

2.5. Biological studies

The cytotoxicity activity of the Ruthenium (II) coordination entities **RuG0, RuG1 and RuG2** was tested against Vero, A549, MCF-7 and HepG2 cell lines by MTT assay and fluorescence assays are done according to reported procedures[53,54] and the detailed experiments are provided in the supplementary information (Section 2.3 to 2.8). The detailed procedure of apoptotic DNA ladder assay of RuG0, RuG1 and RuG2 against HepG2 cell lines are given in the supplementary information (Section 2.9).

Molecular docking studies of the coordination entities **RuG0, RuG1,** and **RuG2** and cisplatin were performed against DNA using Autodock 1.5.6 software, the details of the docking analysis have been provide in the supplementary information (Section 2.10).

3 Results and Discussion

The synthesis of dendrons and ligands was done via the convergent route of dendrimers synthesis methodology, i.e., the synthesis starts from the periphery leading into the core[32,37,55,56]. The detailed procedure is explained in our previous work [36]. The synthesis of **RuG0**, **RuG1,** and **RuG2** involves the reaction between $[Ru(bpy)_2Cl_2.xH_2O]$ and corresponding Gn-bpy (n=0-2) ligands under inert atmosphere. The obtained residue was

purified by column chromatography to obtain **[Ru(bpy)$_2$G0-bpy]Cl$_2$ (RuG0) , [Ru(bpy)$_2$G1-bpy]Cl$_2$ (RuG1),** and **[Ru(bpy)$_2$G2-bpy]Cl$_2$ (RuG2)** coordination entities.

3.1 Characterizations

The spectroscopic characterization of Ru(II) coordination entities is provided in the Supporting Information (**Figures S1** to **S12)**. The FTIR analysis was done for the identification of the functional groups. The prominent functional groups in the synthesized **RuG0, RuG1,** and **RuG2** coordination entities are peripheral methyl groups in the form of esters, the branches' part consists of methylene, aromatic C=C, C-C, ether groups, and finally, the core with aromatic bipyridyl groups. The expected bands and the corresponding functional groups are observed at 2978, 2931 cm^{-1} (for CH_3, C-H Stretching), 1743-1745 cm^{-1} (for C=O stretching (Ester)), 1597-1598 cm^{-1} (for C=C (Aromatic)), 1449-1450 cm^{-1} (for -CH_2- bending), 1370-1371 cm^{-1} (for CH_3, C-H Stretching), 1232-1234 cm^{-1} (for C-O,(Ether), 1139 cm^{-1} (for C-O (Aromatic ether)), ~ 834 cm^{-1} (for C-H (Aromatic)). The ^{1}H-NMR spectra of the coordination entities can be interpreted in four main regions; first, the aromatic protons of the bipyridyl core appear around δ 8.43- δ 7.27 ppm corresponding to six protons, in the second region, the resonance of the aromatic protons of the phenyl branches occur around δ 6.30- δ 6.54 ppm corresponding to a total of 6 (2+4), 18 (6+12) and 38(14+24) aromatic protons of phenyl branches in G0-bpy, G1-bpy and G2-bpy systems respectively. The third region in the ^{1}H-NMR spectra belongs to the methylene -CH_2- proton present at both interior and peripheral ester groups. The resonances for the methylene protons occur between δ 4.43- δ 4.95 ppm, corresponding to a total of 16 (8+8), 32 (4+16+4+8), and 64 (32+8+24) protons of G0-bpy, G1-bpy, and G2-bpy systems respectively. The final region is the most important part, which accounts for the peripheral methyl groups, perhaps the highest peak in every spectrum, the CH_3 protons show sharp a singlet peak centred around δ 1.33- δ 1.48 ppm assigned to the 36, 72 and 144 methyl protons of the synthesized dendritic molecules. The generation wise growth of the prepared dendritic ligands is clear from the observations made in the obtained NMR spectral region between δ 6.30- δ 6.54 ppm (phenyl branches), δ 4.43- δ 4.95 (methylene -CH_2- groups) and δ 1.33- δ 1.48 (methyl CH_3- group). There is a progressive sequential increase in the periphery and inner branches at each layer from generation G0 to G2. The ^{13}C-NMR further substantiates the molecular makeup of the synthesized compounds. The ^{13}C-NMR spectra show expected similarity in each generation of dendron at its associated ligands and coordination entities. The major assignable resonance peaks of the dendrons are of the aryl and methylene carbon at the branches and the *tert*-butyl and carbonyl carbon at the periphery. For the ligands

and coordination entities in addition to what was observed in the case of the dendrons, the ligand showed a signal for the magnetically inequivalent carbon corresponding to the bipyridyl core. The core bipyridine carbon showed a peak around ~159-160 ppm, the carbonyl carbon peak appeared around ~167 ppm, the methyl group appeared around 27-29 ppm, the methylene peak at 65-69 ppm, and the *tert* carbon appeared at ~81 ppm. The mass spectral analysis of the coordination entities has been carried out both by MALDI TOF and ESI MS techniques, however, only the ESI MS spectra are presented in the results. The mass spectral analysis of the coordination entities is quite complicated due to their large size as compared to the dendrons and ligands[57,58]. The low molecular weight **RuG0** has shown $[M\text{-}2PF_6]^{2+}$ ion peak, as the molecular weight of the synthesized coordination entities increases, the fragmentation has become more complicated and intense. For **RuG1** and **RuG2,** the mass spectra exhibit peak corresponding to ions that have undergone fragmentation at dendritic architectures. For **RuG1** the mass spectrum shows a peak corresponding to $[M\text{-}(Cl_2\text{-}8(C_5H_9O_2))^{2+,}$ which is obtained by fragmentation of 8 units of peripheral $C(CH_3)_3COO$ ester groups. The ESI MS spectra of **RuG2** shows a peak corresponding to $[M\text{-}(Cl_2+C_{100}H_{131}O_{31})]^{2+}$ ion formed by the fission of one dendritic arm of the G2-bpy ligand.

3.2 Molecular dynamics studies

The significance of solvating dendritic polymers spans various applications, owing to the profound influence of surface chemistry on the interactions between dendrimers and their environment. Hence, these interactions assume a pivotal role in defining the performance of dendritic polymers.[59] In order to comprehend the atomic-level structure and solvation characteristics of the novel coordination entities, we conducted all-atom molecular dynamics (MD) simulations following the protocols outlined in our previously published research.[32] The simulation details are presented in the Supplementary data, **Section 2**. We examined the behavior, configuration, and size of the coordination entities in both DMSO and water by calculating parameters such as the radius of gyration (Rg) and solvent accessible surface area (SASA) (see the Supplementary data, **Section 2.1 and 2.2** for more details).

Table 1 displays snapshots of the equilibrium conformations of the coordination entities RuG0, **RuG1**, and **RuG2** in both water and DSMO**.** To ascertain whether the system reached an equilibrium state, we analyzed the autocorrelation function of the radius of gyration (R_g) as a function of simulation time ($C_{Rg}(t)$). Additional details can be found in the Supplementary data, **section 2.1**. The data on relaxation time (τ_r) extracted from the $C_{Rg}(t)$ curves indicate that

the simulation durations were sufficiently long to attain equilibrated configurations suitable for modeling the structural and dynamical properties of the dendrons. For further information, please refer to Supplementary data, **Figures S13** and **S14**. It can be observed from **Table 1** that the coordination entities are more extended in DMSO than in water. To quantify this observation, we calculated the Rg and SASA of the coordination entities in the two studied solvents. The data provided in **Table 2** further support the presence of larger-sized structures in DMSO compared to water. This can be attributed to the amphiphilic properties of DMSO, which lead to stronger interactions between DMSO and both the oxygen-containing functional groups (such as ether and ester) as well as the hydrophobic groups (such as methyl and benzene rings) present in the coordination entities. While when placed in water, the coordination entities tend to assume more compact configurations in order to reduce the contact area between their hydrophobic groups and the surrounding water molecules. This behavior is driven by the desire to minimize interactions between the hydrophobic regions and the aqueous environment. We previously observed a similar solvent effect in our research involving ligands of different generations (G0-bpy, G1-bpy, G2-bpy).[32]

We calculated the radial distribution function, g(r), between the dendrons and water as well as between the dendrons and DMSO. Both RDFs can be found in Supplementary data, **Figures S15(a)** and **S15(b)**, respectively. In systems involving water, the first peaks of the RDFs occurred at shorter distances than those in DMSO. This discrepancy can likely be attributed to the smaller size of water molecules compared to DMSO molecules. Additionally, the higher values of g(r) observed in the systems containing DMSO provide further evidence that the dendrons exhibit greater compatibility with DMSO compared to water. This observation aligns with the R_g data presented in **Table 2**, supporting that DMSO is a more favorable solvent for these dendrons.The SASA values reported in **Table 2** also confirm that the dendron structures in DMSO are indeed larger than those in water. This supports the earlier observations of greater extension and compatibility of the dendrons in DMSO. **Figures S15 (c)** and **(d)** illustrate the $g(r)$ between the dendrons' oxygen atoms and the solvents' oxygen atoms, which also confirms the better compatibility of the coordination entities with DMSO than water.

Table 1 Snapshots capturing the equilibrium conformations of the investigated Ruthenium (II) coordination entities in both water and DMSO. Carbon, oxygen, nitrogen, hydrogen, and ruthenium atoms are represented in grey, red, blue, white, and green, respectively.

Coordination entities	WATER	DMSO
RuG0	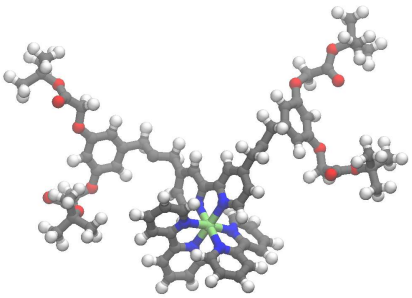	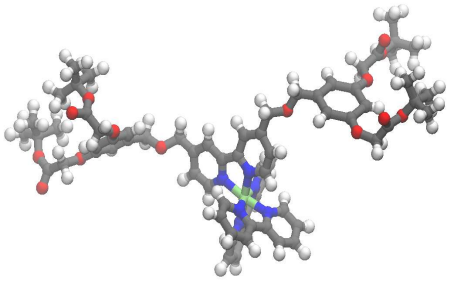
RuG1	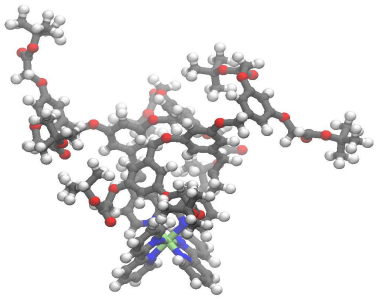	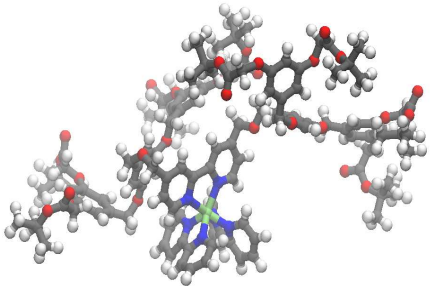
RuG2	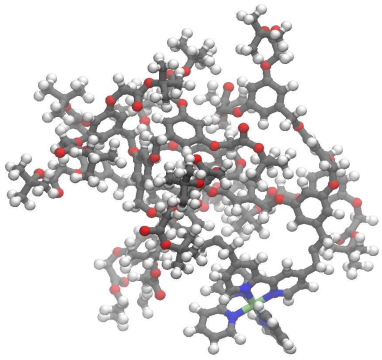	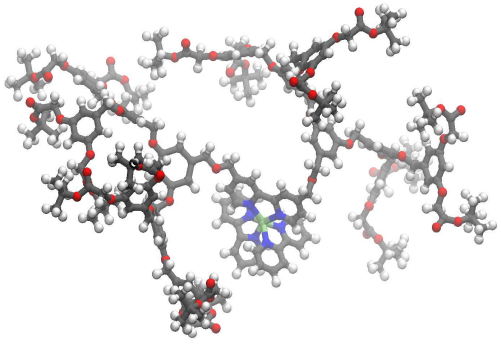

Table 2 Calculated R_g and SASA of ruthenium (II) coordination entities in water and DMSO. The results of the R_g and SASA were obtained by averaging data across the sampled data (from the last 7 ns of each simulation; the selected frames were 500 ps apart) of each simulation run.

Coordination entities	Water		DMSO	
	R_g (Å)	SASA (Å^2)	R_g (Å)	SASA (Å^2)
RuG0	12.21 ± 1.5	3430.40 ± 51.53	14.85 ± 1.03	8290.82 ± 114.04
RuG1	12.57 ± 1.08	3201.30 ± 41.10	17.09 ± 3.32	9271.42 ± 64.14
RuG2	19.84 ± 3.54	3536.39 ± 61.45	21.14 ± 3.22	10141.02 ± 84.45

3.3. Cytotoxicity studies by MTT assay

In vitro cytotoxicity studies on A549 lung adenocarcinoma cell line, MDA MB 231 human breast epithelial adenocarcinoma cell lines, HepG2 liver cancer cell, and normal kidney epithelial cell line Vero of the ruthenium(II) coordination entities **RuG0, RuG1,** and **RuG2** by MTT assay were performed. The coordination entities have shown a concentration dependent cytotoxicity against the cancerous cell lines A549, MDA MB 231, and HepG2 cells and non-cancerous Vero cell line shown in **Figure 3.** The IC_{50} value of the cytotoxicity of **RuG0, RuG1 and RuG2,** and cisplatin are shown in **Table 3.**

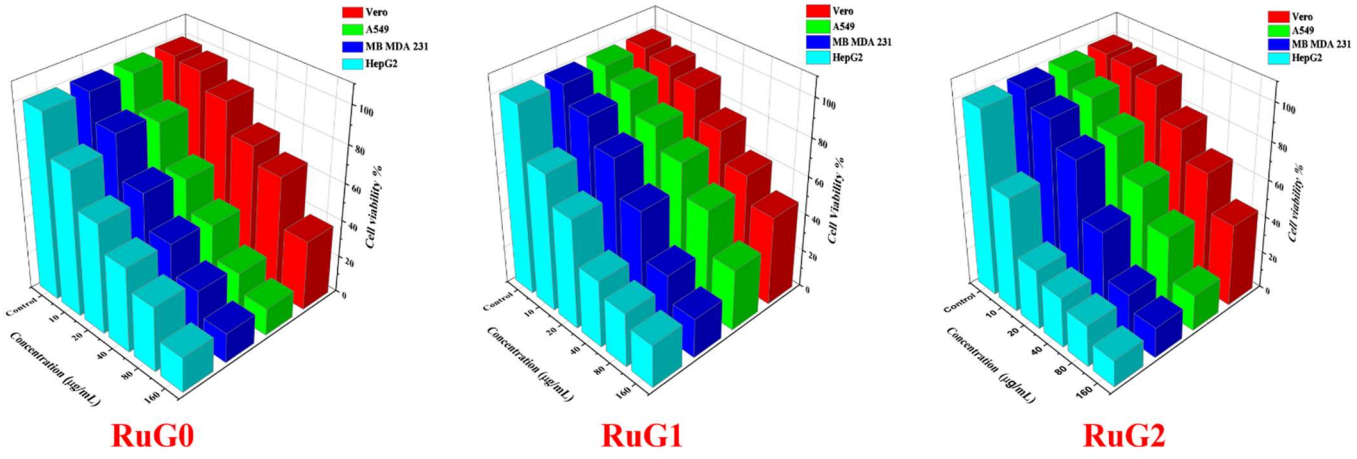

Figure 3 *In vitro* cytotoxicity of **RuG0, RuG1,** and **RuG2** against Normal cell line Vero (Red), A549 lung cancer cell line (Green), MDA MB 231 human breast cancer cell lines (Dark Blue), HepG2 liver cancer cell (Cyan) by MTT assay.

Table 3 The cytotoxic IC_{50} concentrations (μg/mL ± SD) of **RuG0, RuG1, RuG2** and cisplatin against the Vero, A549, MDA MB 231, and HepG2 cell lines

Coordination entities	Vero	A549	MDA MB 231	Hep G2
RuG0	111.90 ± 4.85	30.52 ± 1.12	35.50±1.80	34.88 ± 3.28
RuG1	135.16 ± 6.14	89.76 ± 1.72	52.13±1.75	27.77 ± 0.41
RuG2	112.8 ± 1.21	58.75 ± 1.73	41.98±1.18	13.15 ± 0.51
cisplatin	-	23.42±0.21	28.77±0.22	9.74 ± 0.32

It can be concluded from **Table 3** that the **RuG0, RuG1,** and **RuG2** are highly cytotoxic against the three cancer cell lines, with the highest activity observed against the HepG2 liver cancer cell and very mildly cytotoxic against the normal vero cell lines. Among the A549 cell line, coordination entities **RuG0** exhibited highest activity with an IC_{50} concentration of 30.52±1.12μg/mL, while **RuG1** exhibited the lowest activity with an IC_{50} concentration 89.76 ± 1.72μg/mL. In MDA MB 231 cell lines the highest and lowest activity was exhibited by **RuG0** and **RuG1** with an IC_{50} concentration of 35.50±1.80μg/mL and 52.13±1.75μg/mL, respectively. The observed trend in the cytotoxicity can be explained based on the influence of both, the accessibility of Ru(II) ions and the dendrimeric effect. **RuG0** containing lower generation G0-bpy ligand exposes the Ru(II) ions to the tumorous cells and induce cytotoxicity more effectively than the higher generation analogous ligands, **RuG2** with higher molecular weight containing and having G2-bpy ligand, with heavy steric crowding, restricts the Ru(II) ion interaction with the cell lines and hence exhibit lower cytotoxicity among the series.

The HepG2 liver cancer cell, unlike the A549 and MDA MB 231, has shown linear relation with the cytotoxic effect and size of ligands from G0-bpy to G2-bpy. The highest cytotoxicity has been shown by **RuG2**, with an IC_{50} concentration of 13.15 ± 0.51μg/mL, from the Table 3, it's found that the IC_{50} concentrations have decreased from **RuG0** to **RuG1,** at higher generation coordination entities **RuG2**, the influence of ligand size and more number of surface groups have induced the cytotoxicity in the cell lines. Coordination entities **RuG2** incorporated with a large number of *tert* butyl group is superior to the other synthesized coordination entities in antiproliferation. The higher electron donating nature of the G2-bpy ligand enhances the lipophilic character of the coordination entity and facilitating its penetration across the lipid cell membrane[54,60,61]. Further, there are reports on the higher generation of dendrimers inducing higher cytotoxicity in HepG2 cell lines, by cellular internalisation followed by faster and

stronger endocytosis compared to other cell lines[18,19]. All the synthesized Ru(II) coordination entities have exhibited lower cytotoxicity, of an IC_{50} concentration >100 μg/mL, towards the non-cancerous normal cell lines, which infers the selectivity of the Ru(II) coordination entities towards cancerous cell line more than the normal cells. In conclusion, the finding emphasizes the importance of the synthesized coordination entities as potential candidates exhibiting anticancer activity with minimal side effects in comparison to cisplatin.

3.4. Fluorescence imaging studies

3.4.1. Apoptotic morphological analysis by Acridine orange/Ethidium bromide dual staining

The cells were cultured in a 6-well plate (1×10^5 cells per well) and treated with IC_{50} concentration of **RuG0, RuG1,** and **RuG2** for 24 h. The untreated cells served as a control. After the treatment, the stained cells were observed and examined under a fluorescence microscope(Invitrogen EVOS FL cell imaging; 40xmagnification). Acridine Orange−Ethidium Bromide (AO/EB) staining is fluorescence based double staining technique used to distinguish between live and dead cells. Acridine orange and ethidium bromide are DNA intercalators that bind to the DNA of live and dead cells, respectively. In this method, acridine organge is used to stain both viable and dead cells, while cells with damaged membranes are stained by ethidium bromide. Under a fluorescence microscope, live cells appear as green, while necrotic cells stain red, however, their nuclear shape remains alike of live cells. Apoptotic cells, on the other hand, manifest as greenish-orange patches, reflecting the morphological changes associated with apoptosis. AO/EB allows simultaneous assessment of both live and dead cells, and determination of the efficacy of drug treatments on cell viability. Induction of apoptosis on selective or targeted cancer cells is a key role of therapeutic anticancer agents. Apoptosis involves characteristic phenotypical changes in cell morphology, which includes cell shrinkage of the cytoplasm, nuclear condensation, plasma membrane blebbing, DNA fragmentation, and phosphatidylserine translocation to the extracellular sides[53]. Apoptotic cell death mechanism by the AO/EB staining assay of **RuG0, RuG1,** and **RuG2** in A549, MDA MB 231, and HepG2 cells are shown in **Figure 4**, **Figure S16,** and **S17** respectively. As illustrated in the fluorescence microscopy images of Ru(II) coordination entities treated cells, the AO/EB staining clearly indicates that the coordination entities have induced apoptosis in the respective cell lines[60–64] As evident for from MTT assay, The AO/EB fluorescence microscopy images of HepG2 cell lines have shown higher apoptosis with the prepared coordination entities.

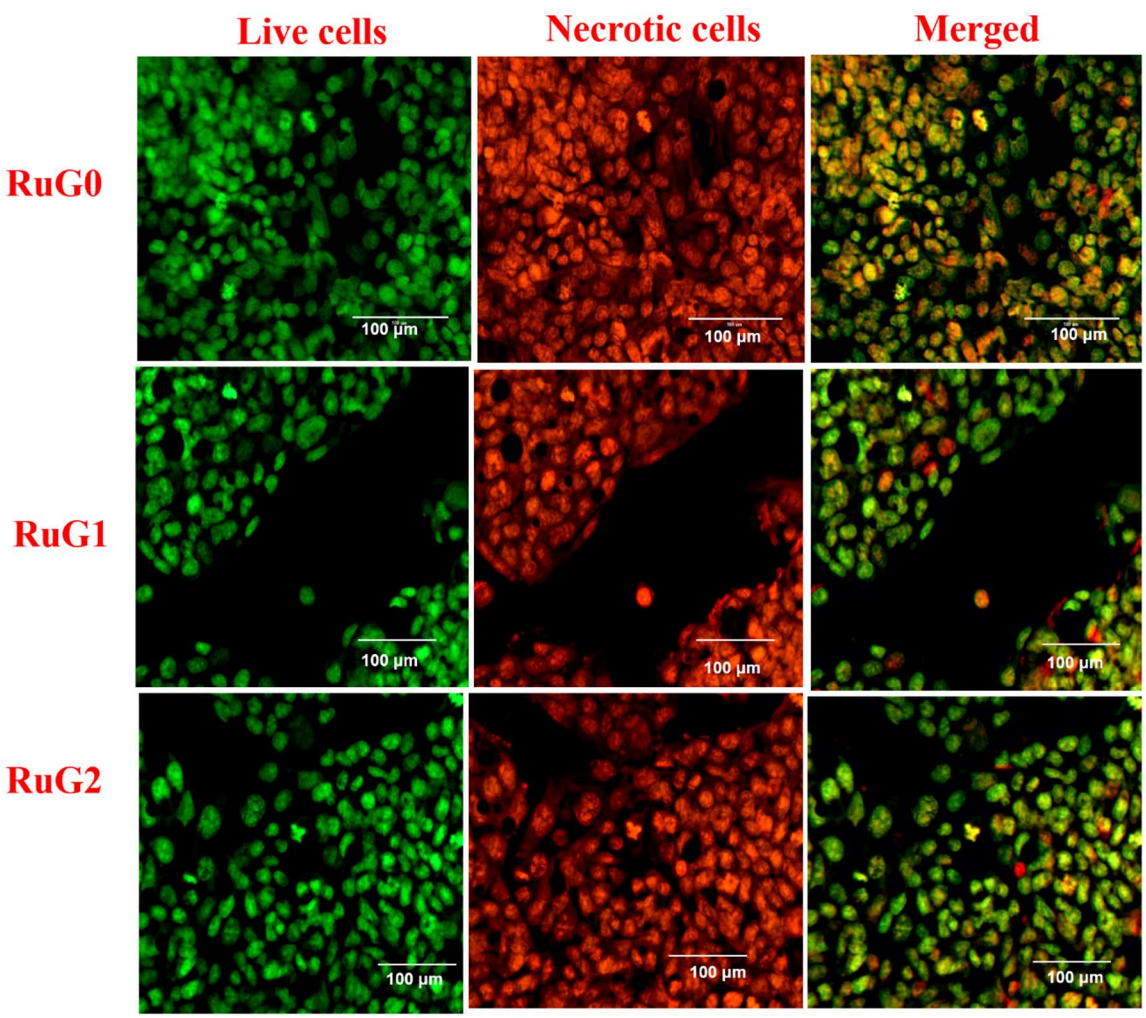

Figure 4 Apoptotic cell death mechanism by the AO/EB staining assay by **RuG0, RuG1,** and **RuG2** at the IC_{50} in HepG2 cells for 24 h (Magnification: 40x, scale bar 100 µm) a) live cells b) necrotic cells c) merged

3.4.2. Nuclear morphology analysis by DAPI staining

The (4',6-diamidino-2-phenylindole) or DAPI assay is a versatile fluorescence staining tool to quantify DNA content, fragmentation, and DNA damages in a cell. Typically, the DAPI assay uses 4',6-diamidino-2-phenylindole, a fluorescence dye which preferentially binds to the AT regions of DNA and shows bright blue emission allowing it to view under a fluorescence microscope. The intensity of the blue emission is directly proportional to the DNA present in the cell. Further, the irregularity in the fluorescence image pattern and the strongly intense blue spots concludes the presence of DNA damage or fragmentation[53]. The DAPI analysis validates cell death phenomena that could have occurred due to apoptosis or cytosis induced by the coordination entities. **Figure 5, Figures S18,** and **S19** show the nuclear morphology analysis by DAPI staining assay on A549, MDA MB 231, and HepG2 cells by **RuG0, RuG1,** and **RuG2**, respectively. In all the cell lines, the coordination entity untreated cell lines have not

shown any blue stains caused by DAPI, as the cells are intact, and the DAPI could not have bound with DNA of the cell. While in the case of coordination entity treated cell lines, the cells might lose its structural integrity and expose the fragmented DNA or the damaged DNA. The DAPI now binds effectively with the DNA fragments and stains it. The DAPI analysis of the **RuG0, RuG1**, and **RuG2** clearly shows a higher degree of DNA damage in all three cell lines as the ligand size increases. From the DAPI analysis, it can be concluded that the dendrimeric coordination entities clearly induce cell death by necrosis due to ligands and Ru(II) induced apoptosis. The highest damage is shown by HepG2 cell lines which coincide with findings of MTT assays.

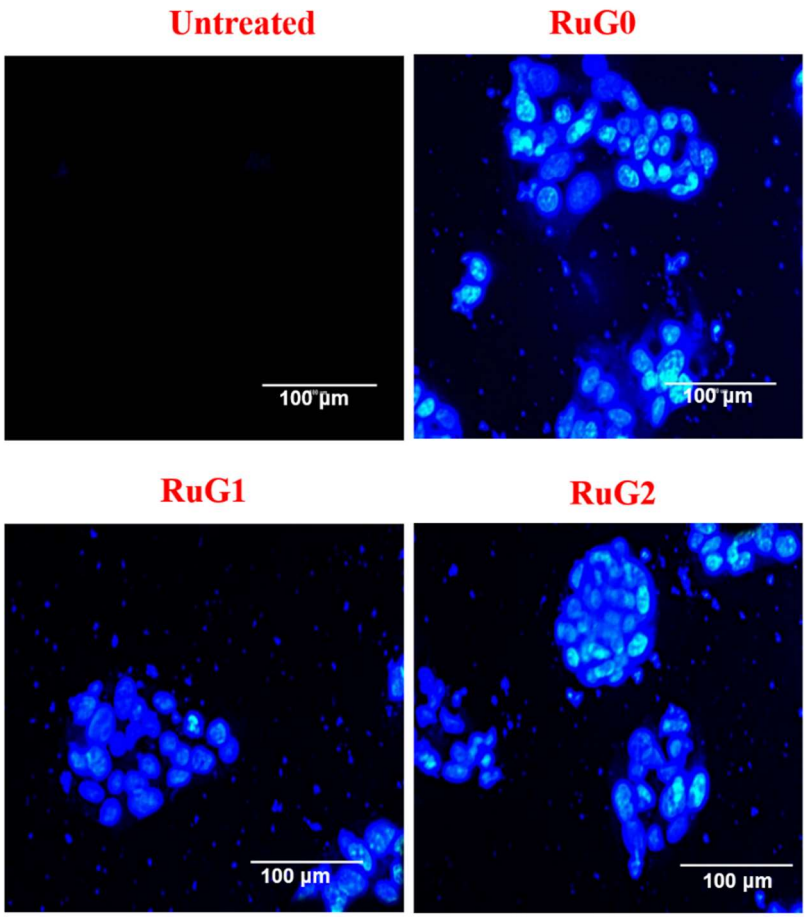

Figure 5 Nuclear morphology analysis by DAPI staining assay on HepG2 cells by coordination entities **RuG0, RuG1**, and **RuG2** at the IC_{50} (Magnification: 40x, scale bar: 100 µm)

3.4.3. Cell death analysis by propidium iodide (PI) assay

The cultured cells in a 6-well plate (1×10^5 cells per well) were treated with IC_{50} concentration of **RuG0, RuG1,** and **RuG2** and incubated for 24 h. The fluorescence microscope was used to observe the nucleus of the cells undergoing late stage apoptosis or

exhibiting the characetistics of necrosis. **Figure 6, Figure S20,** and **S21** show the cell death analysis of A549, MDA MB 231 and HepG2 cells by **RuG0, RuG1,** and **RuG2,** respectively. Propidium iodide – PI staining is a widely used protocol to determine or quantify late apoptotic and necrotic cells. Propidium iodide is a DNA binding dye that intercalates between the bases with little or no sequence preferences, upon binding of PI dye, it emits strong red fluorescence which is viewed under a microscope. The PI assays help to predict the necrosis based anticancer mechanism. The ability of PI to stain the cells depends upon the integrity of its cell membrane, therefore, PI cannot stain a live or early apoptotic cells.[65] This is clearly evident from the coordination entity untreated control experiments, wherein very little or no red stains are observed; this indicates that the cell membranes are intact and do not allow the passage of PI. In cases of **RuG0, RuG1,** and **RuG2** treated cells lines stronger red images are observed indicating the presence of death cells, it is clearly concluded that on treatment with the coordination entities the integrity of the cell membrane is lost, and PI very well gets access to the DNA molecules, and emit strong red fluorescence.

The cell death analysis can be quantified based on the red emission intensity profile, shown in **Figure 7.** The fluorescence intensity profile shows higher cell death in MDA MB 231 compared to A549 and HepG2 cells in all three coordination entities. Coordination entities **RuG0**, has exhibited higher cell death in all three cell lines; this may infer that **RuG0** disrupts the cell membrane and induces cell death by a necrosis mechanism compared to other coordination complexes.[66]

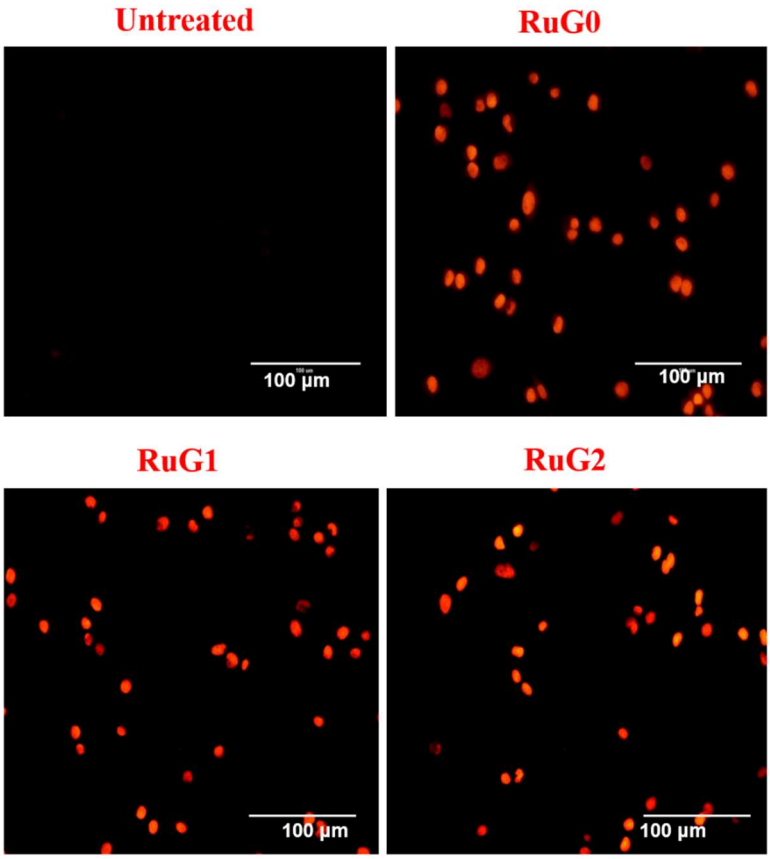

Figure 6 Cell death analysis by propidium iodide- PI staining assay on MDA MB 231 cells by **RuG0, RuG1,** and **RuG2** at the IC_{50} concentration (Magnification: 40x, scale bar: 100 µm)

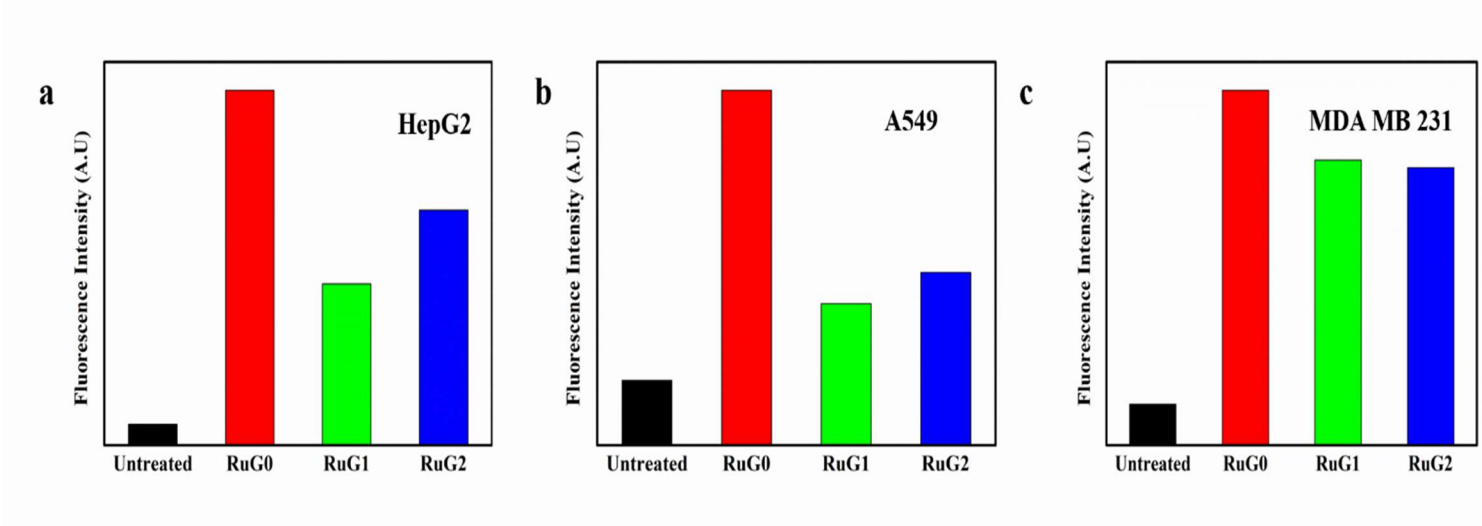

Figure 7 Quantification of cell death in a) HepG2 b) A549 and c) MDA MB 231 cell lines induced by **RuG0, RuG1,** and **RuG2** via propidium iodide- PI staining assay.

3.4.4 Analysis of mitochondrial membrane potential ($\Delta\psi_m$)

The mitochondrial membrane integrity is an essential factor that has to be maintained for sustained cellular level functions. Cell death can be induced in tumours by disrupting the mitochondrial functions; typically this happens when an anticancer agent enters the cell and disrupts the mitochondrial membrane, thereby inducing apoptosis[67]. Mitochondrial membrane potential is an indicator of membrane integrity which can be determined by fluorescence assay, using Rhodamine 123 dye. Rhodamine 123 dye is cationic dye which preferentially accumulates on the negatively charged mitochondrial membrane and stains the mitochondria in the membrane potential-dependent manner. Any disruption in the membrane by the ruthenium coordination entities would change the mitochondrial membrane potential, which alters the fluorescence of the Rhodamine dye[68]. The fluorescence intensity of the dye serve as a distinguish factor to evaluate the mitochondrial functions between the treated and untreated cancer cells. **Figure 8** and **Figure S22** to **S23** shows rhodamine 123 staining of A549, MDA MB 231, and HepG2 cells with coordination entities **RuG0, RuG1,** and **RuG2** at the IC_{50} concentration, respectively. The control cells, with bright green fluorescence, show that they are undamaged cancerous cells. Upon treatment of cells with the synthesized coordination entities, a reduction in the fluorescence intensity is observed. The decrease in the fluorescence instensity serve as a quantitative measure of the extent of apoptosis, as it corresponds to a reduction in membrane potential compared to the control group, as shown in **Figure 9.**

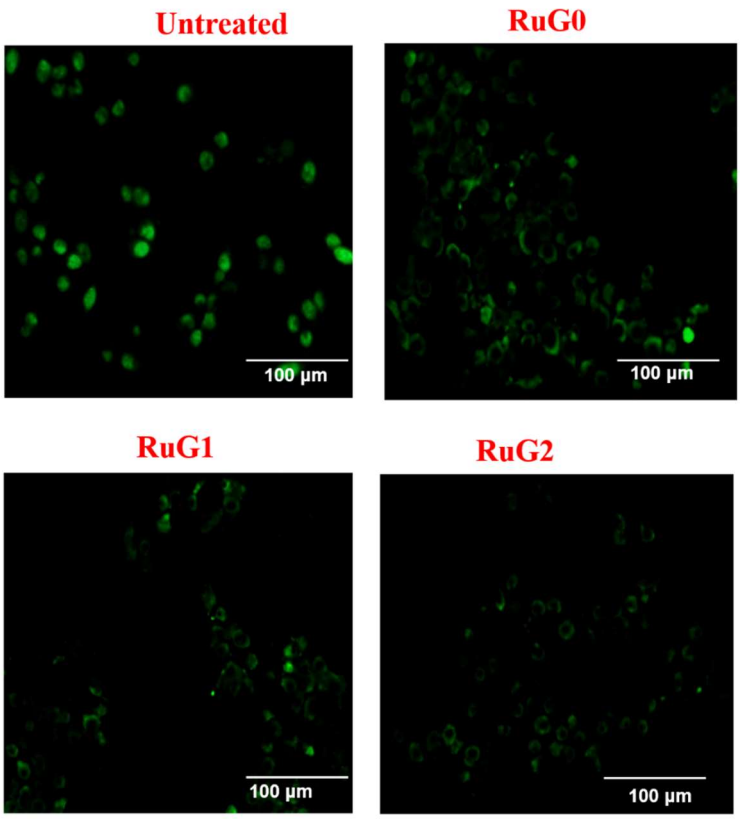

Figure 8 Rhodamine 123 staining of HepG2 cells with Ru(II)- coordination entities at the IC_{50} concentration (Magnification: 40x, scale bar: 100 µm)

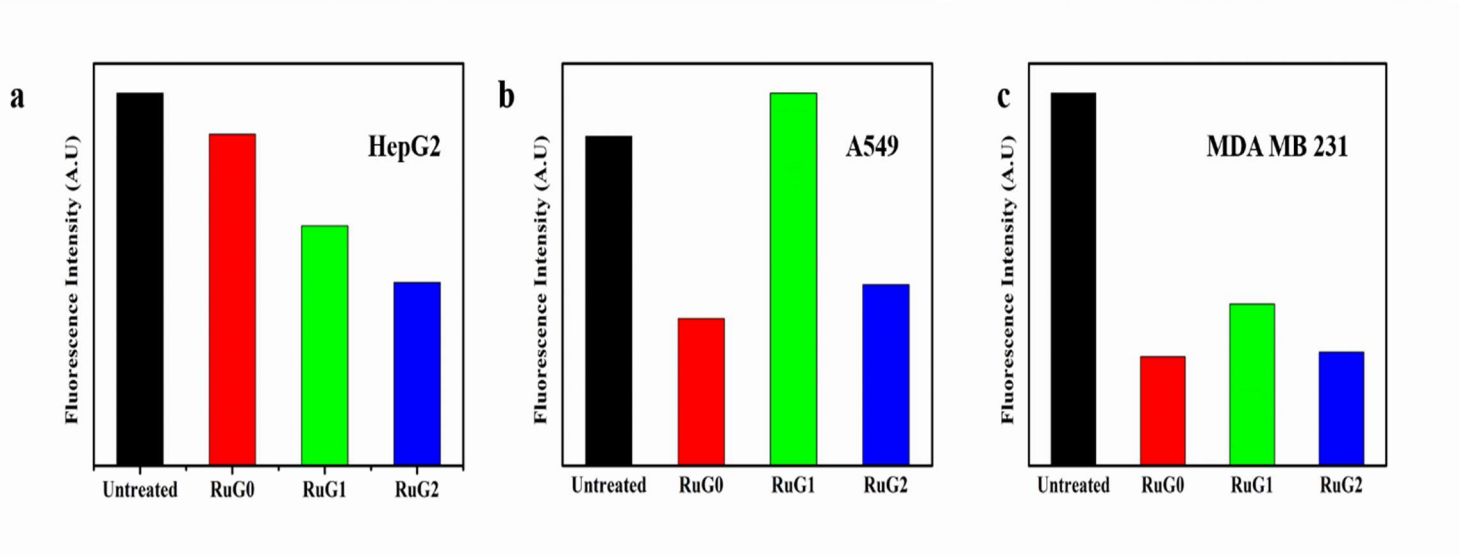

Figure 9 Quantification of mitochondrial membrane potential ($\Delta\psi_m$) a) HepG2 b) A549 and c) MDA MB 231 cell lines with Ru(II)- coordination entities

3.4.5 Reactive Oxygen Species (ROS) Assay

ROS are known for their strong cytocidal properties; often generation of ROS at the cancerous cell is considered as a pathway in the cure of cancer. Anticancer drugs such as cisplatin, doxorubicin and paclitaxel etc., have been known to induce ROS generation in cancerous cells leading to oxidative stress and subsequently to their death. The production of ROS may be due to the inhibition of antioxidant mechanism or mitochondrial dysfunction induced by the drug in cancerous cells. Therefore, the assessment of ROS in a cancerous cell line is a method to evaluate their anticancer potency of any drug. There are numerous reports on the capability of ROS generation by ruthenium coordination entities, making them ideal candidates as anticancer agents[69–71]. The ROS assay is a fluorescence staining protocol that uses DCFH-DA (2,7-Dichlorodihydrofluorescein diacetate). This nonpolar non fluorescent dye undergoes oxidation in the presence of cytoplasmic ROS (generated by the drug) to form DCF (2,7-Dichlorodihydrofluorescein), which exhibits strong fluorescence. The intensity of fluorescence is directly proportional to the ROS generated and the efficiency of the anticancer drug. **Figure 10** and **Figure S24** to **S25** shows the ROS detected in IC_{50} dose of **RuG0, RuG1,** and **RuG2** coordination entities treated A549, MDA MB 231, and HepG2 cell line, respectively. It is observed from the fluorescence microscopic images that the three cell lines have strong ROS production in the presence of the prepared dendrimeric Ru(II) coordination entities compared to the untreated cell lines. From **Figure 11**, it is determined that **RuG2** with a larger number of electron donating groups around the Ru(II) has shown relatively higher ROS generation against A549 HepG2 cell lines, while in the case of MDA MB 231 **RuG0** has shown a higher degree of ROS genearation[72,73].

On the basis of chemotherapeutic approach ruthenium(II) coordination entities can generate ROS by several mechanisms, namely the mitochondria mediated pathway, the DNA damage-mediated pathway, and the death receptor-mediated pathway[74,75]. From all previous staining protocols, it is evident that the synthesized coordination entities are exhibiting their anticancer characteristic following one or more aforementioned pathways.

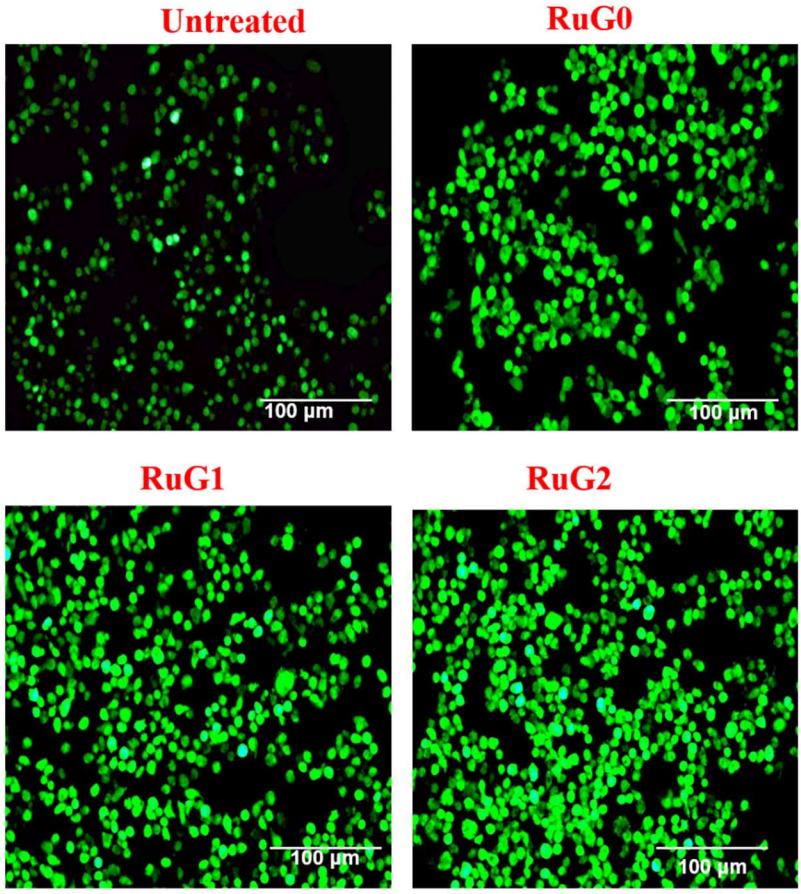

Figure 10 ROS detection on HepG2 cells by Ru(II)- coordination entities s at the IC_{50} concentration (Magnification: 40x, scale bar: 100 µm)

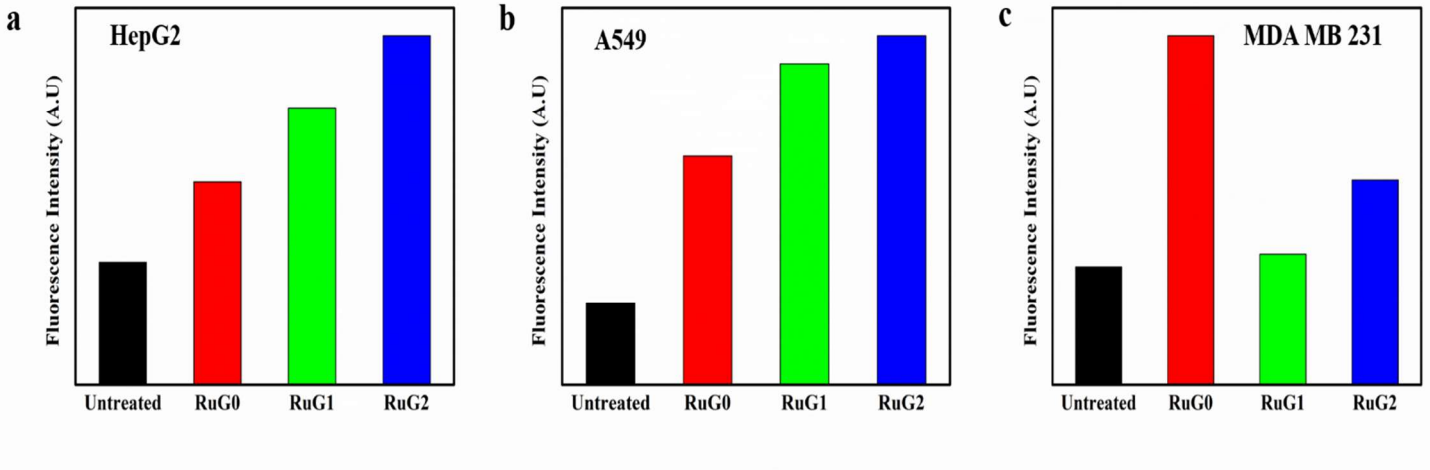

Figure 11 Quantification of ROS detection on) a) HepG2 b) A549 and c) MDA MB 231 cell lines with Ru(II)- coordination entities

3.5 DNA Ladder Assay.

The DNA ladder assay was performed on the HepG2 cell lines, DNA laddering is a characteristic feature of the DNA degradation mediated by the caspase-activated DNase (CAD), which represents a pivotal event in the process of apoptosis. DNA fragmentation refers to the cleavage of chromosomal DNA at specific internucleosomal sites into several units, typically in the range of 180–200 base pair fragments. These fragments, when visualized through gel electrophoressis, exhibit a distinct "ladder" pattern, owing to their separation during agarose gel electrophoresis.

The HepG2 cell lines were incubated with IC_{50} concentrations of the coordination entities **RuG0, RuG1** and **RuG2** in DMEM culture medium at 37 ºC for 24 h. Subsequently, DNA fragments were isolated from both the treated and control samples and these samples are are subjected to 1.2% agarose gel electrophoresis. The resulting gel was photographed using a gel documentation system. The photographed images of both the test samples exhibit the ladder formation (lane 3, 4 and 5 in **Figure 12**) demonstrating cell apoptosis, whereas the DNA isolated from the control HepG2 cells does not exhibit any ladder formation. These findings collectively suggests that the coordination entities have the ability to promote apoptosis in HepG2 cell lines lending support for their antitumor activity.

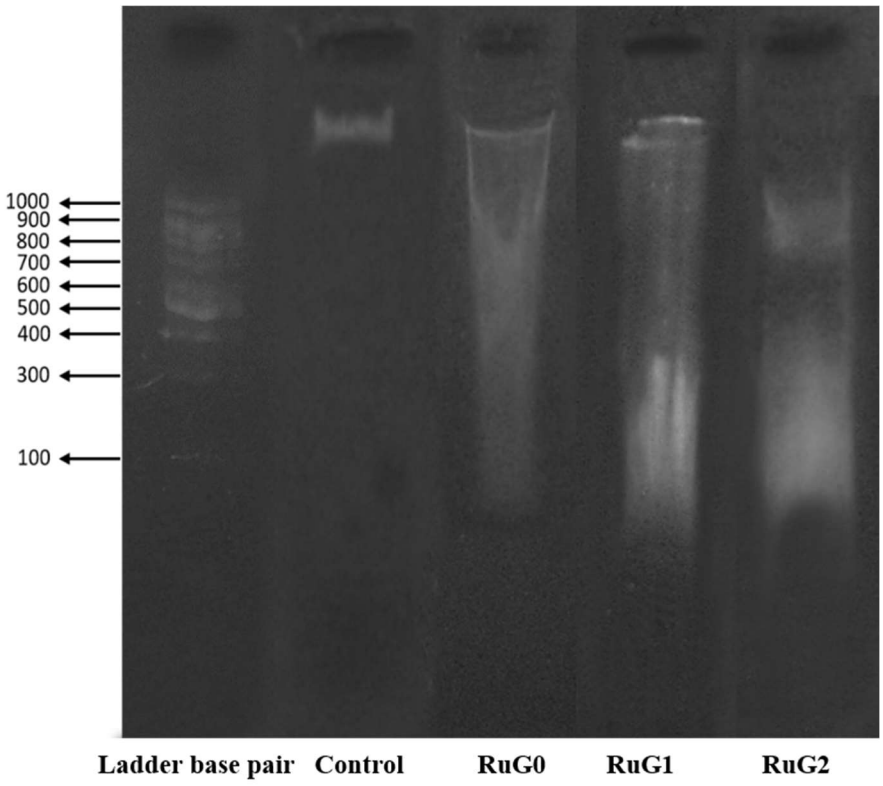

Figure 12 DNA ladder assay in HepG2 cells. Lane 1: Base pair ladder; Lane 2: control DNA, Lane 3, 4 and 5 are IC_{50} concentration **RuG0,RuG1** and **RuG2** treated DNA.

3.6 Molecular Docking analysis with DNA

Polypyridyl-based ruthenium(II) coordination entities have shown strong affinity to DNA, both covalently and non-covalently [76]. In recent years, researchers have become interested in determining the binding sites of metallodrugs to biomolecules. There are several studies done on the DNA binding potential of Ru(II) coordination entities, the extend of binding depends upon the constitution of ligands[77–79]. DNA binding can happen in two ways, the coordination entities can either bind by intercalation or groove binding. Hence the molecular docking analysis was carried out to predict the binding energy and binding pockets. To predict the possibility of intercalation 1Z3F (DNA with intercalation gap) was used for docking purposes. On the other hand, the possibility of intercalation, groove binding was predicted using the DNA with a canonical gap of 1BNA[80]. The lowest-energy docked poses of **RuG0, RuG1,** and **RuG2** and cisplatin with both types of DNA (1Z3F and 1BNA) are illustrated in **Figure 13** and **Figure 14.** The docking binding energy of both types of DNA is shown in **Table 4** and **Table 5**. It is found that for **RuG0**, with G0-bpy ligand, the binding energy in DNA intercalation gap is higher than DNA with a canonical gap. While in the case of cisplatin, **RuG1,** and **RuG2** the binding energy is found to be higher for DNA with canonical gaps, thus it can be predicted in **RuG0** groove binding is more favourable.

Table 4 Binding energy and interacting residues for the molecular docking analysis of the **RuG0, RuG1,** and **RuG2** and cisplatin with DNA (PDB ID: 1Z3F)

PDB ID	**Coordination entities**	**Binding energy in kcal mol^{-1}**	**Interacting Residues**
1Z3F – DNA with intercalation gap	RuG0	-7.6	DA5, DT1
	RuG1	-5.0	DA5, DT1
	RuG2	-5.4	DA5, DT1
	cisplatin	-3.1	DA5, DT1

Table 5 Binding energy and interacting residues for the molecular docking analysis of the **RuG0, RuG1, RuG2** and cisplatin with DNA (PDB ID: 1BNA)

PDB ID	**Coordination entities**	**Binding energy in kcal mol^{-1}**	**Interacting Residues**
1BNA– DNA with canonical gap	RuG0	-6.7	DC21,DT20,DT19,DA18,DG3 ,DG2,DC1,DA6
	RuG1	-6.0	DA5,DG4,DC3,DG2,DC21,DT20
	RuG2	-5.8	DC1, DG24, DC20
	cisplatin	**-3.7**	DT20, DT19, DA18,DT7,DT8

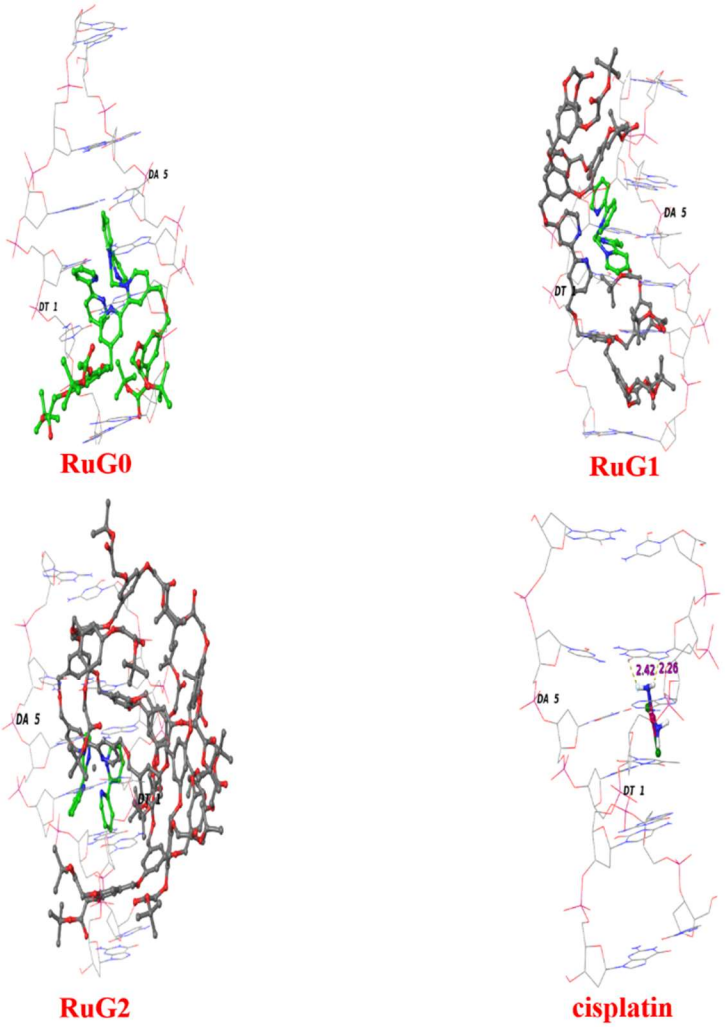

Figure 13 3D docking illustration of **RuG0, RuG1, RuG2** and cisplatin with DNA of the intercalation gap (PDB ID 1Z3F)

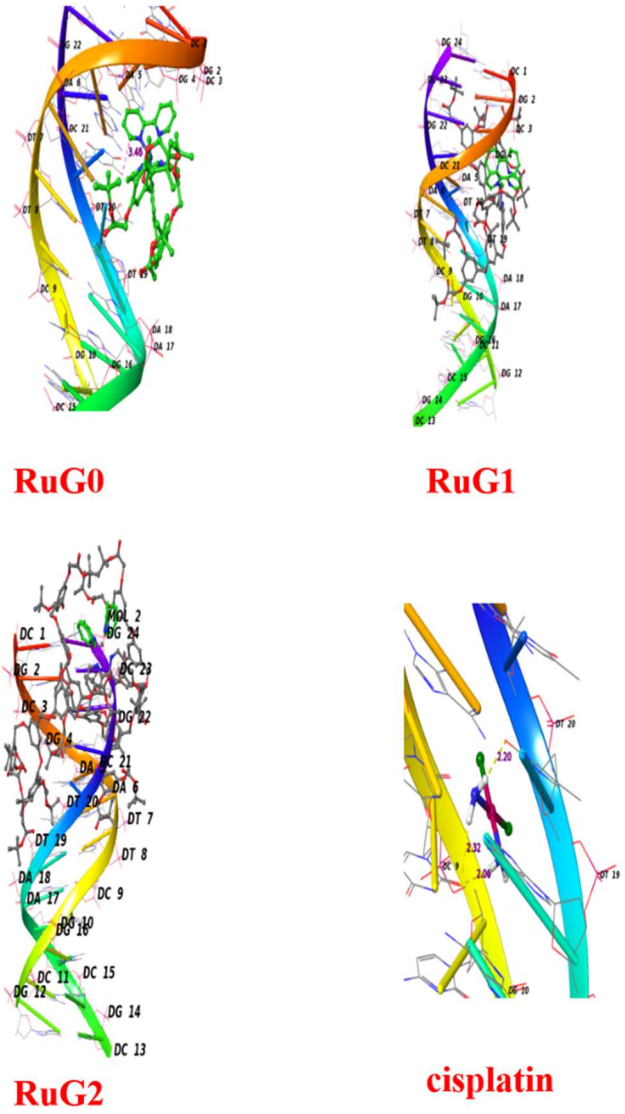

Figure 14 3D docking illustration of **RuG0, RuG1, RuG2** and cisplatin with DNA of the canonical gap (PDB ID 1BNA)

4. Conclusion

The dendritic poly(aryl ether) substituted polypyridyl ligands-based ruthenium(II)-coordination entities, **RuG0, RuG1,** and **RuG2** were synthesized and characterized with various spectroscopic tools such as IR, NMR, and mass spectroscopy. Molecular simulation studies were performed to determine the solvent dependent behaviour of the coordination entities.

The three coordination entities **RuG0, RuG1,** and **RuG2** displayed cytotoxicity against various cancer cell lines A549, MDA MB 231, and HepG2 cancerous cells. **RuG0** exhibited higher

potency against A549 and MDA MB 231 cell lines while interestingly, the dendritic complexes showed generation-dependent cytotoxicity, that is the cytotoxicity of coordination entities varied based on the generation of the dendritic ligand structure (G0-bpy, G1-bpy and G2-bpy), against HepG2 cancerous cells only. The AO/EB and DAPI fluorescent staining study confirm that the titled coordination entities trigger apoptosis in HepG2 cells. The cell death analysis by propidium iodide- PI staining study confirms that **RuG0** disrupts the cell membrane and induces cell death by a necrosis mechanism compared to other coordination entities. Further, the mitochondrial membrane potential measurement and ROS assay validate that the dendritic coordination entities induce oxidative stress and subsequent apoptosis in the cancerous cells by disrupting mitochondrial membrane integrity and generation of intracellular ROS, respectively. The results of DNA ladder assay and molecular docking anlysis helps to understand the interactions with DNA. Based on the above experimental results, it can be concluded that the dendritic poly(aryl ether) substituted polypyridyl ligands-based Ruthenium(II)-coordination entities with the biologically suitable chelating ligands can be a suitable platform for developing new anticancer agents.

Supplementary Information: The ^{1}H-NMR, ^{13}C-NMR, and mass spectra of the synthesized Ru(II) coordination entities are provided in **Figures S1 – S12.** Models and simulation details of ruthenium (II) coordination entities of G0-bpy, G1-bpy, and G2-bpy are shown in **Table S1** and **Figures S13-S15.** All Fluorescence imaging studies of cell lines A549 and MDA MB 231 are provided in **S16 – S25**.

Acknowledgment

L.R and E.R acknowledges the Science and Engineering Research Board Department of Science and Technology (DST-SERB), for the funding under the Young Scientist Scheme CS155/2013. We acknowledge SAIF-IIT Madras for the HR-MS and ESI-MS analysis. L.R acknowledge SRM Institute of Science and Technology for the NMR analysis. L.R acknowledges Mr Priya Ranjan Dev for the preprartion of manuscript graphical abstract. S.J.N. and M.V. acknowledge the Irish Centre for High-End Computing (ICHEC) for the computational facilities and support. This work was supported by the European Union's Horizon 2020 research and innovation programme under the Marie Skłodowska-Curie grant to S.J.N., Agreement No. 847402 (Project ID: MF20210297).

Author Details

Liju Raju

Department of Chemistry, Madras Christian College (Autonomous), Affiliated to the University of Madras, Tambaram East, Chennai, Tamilnadu, India 600059.

https://orcid.org/0000-0001-9812-1721

Sousa Javan Nikkhah

Department of Chemical Sciences and Bernal Institute, University of Limerick,Limerick V94 T9PX, Republic of Ireland

https://orcid.org/0000-0003-1725-4069

MosaChristas K

Department of Plant Biology and Biotechnology & Loyola Institute of Frontier Energy (LIFE), Loyola College (Autonomous), University of Madras, Chennai, India 600034

https://orcid.org/0000-0003-2210-6458

Matthias Vandichel

Department of Chemical Sciences and Bernal Institute, University of Limerick,Limerick V94 T9PX, Republic of Ireland

https://orcid.org/0000-0003-1592-0726

Corresponding Author

Eswaran Rajkumar

Department of Chemistry, Madras Christian College (Autonomous), Affiliated to the University of Madras, Tambaram East, Chennai, Tamilnadu, India 600059.

https://orcid.org/0000-0001-6194-8696

Email: rajjkumar@gmail.com

Conflict of interest

There are no conflicts to declare.

References

(1) Parveen, S. Recent Advances in Anticancer Ruthenium Schiff Base Complexes. *Appl. Organomet. Chem.* **2020**, *34* (8), e5687. https://doi.org/10.1002/aoc.5687.

(2) Shen, J.; Rees, T. W.; Ji, L.; Chao, H. Recent Advances in Ruthenium(II) and Iridium(III) Complexes Containing Nanosystems for Cancer Treatment and Bioimaging. *Coord. Chem. Rev.* **2021**, *443*, 214016. https://doi.org/10.1016/j.ccr.2021.214016.

(3) Coverdale, J. P. C.; Laroiya-McCarron, T.; Romero-Canelón, I. Designing Ruthenium Anticancer Drugs: What Have We Learnt from the Key Drug Candidates? *Inorganics* **2019**, *7* (3), 31. https://doi.org/10.3390/inorganics7030031.

(4) Sanna, V.; Pala, N.; Sechi, M. Targeted Therapy Using Nanotechnology: Focus on Cancer. *Int. J. Nanomedicine* **2014**, *9*, 467–483. https://doi.org/10.2147/IJN.S36654.

(5) Yao, Y.; Zhou, Y.; Liu, L.; Xu, Y.; Chen, Q.; Wang, Y.; Wu, S.; Deng, Y.; Zhang, J.; Shao, A. Nanoparticle-Based Drug Delivery in Cancer Therapy and Its Role in Overcoming Drug Resistance. *Front. Mol. Biosci.* **2020**, *7*, 193. https://doi.org/10.3389/fmolb.2020.00193.

(6) Cheng, Z.; Li, M.; Dey, R.; Chen, Y. Nanomaterials for Cancer Therapy: Current Progress and Perspectives. *J. Hematol. Oncol.J Hematol Oncol* **2021**, *14* (1), 85. https://doi.org/10.1186/s13045-021-01096-0.

(7) Spreckelmeyer, S.; Orvig, C.; Casini, A. Cellular Transport Mechanisms of Cytotoxic Metallodrugs: An Overview beyond Cisplatin. *Molecules* **2014**, *19* (10), 15584–15610. https://doi.org/10.3390/molecules191015584.

(8) Novohradsky, V.; Liu, Z.; Vojtiskova, M.; Sadler, P. J.; Brabec, V.; Kasparkova, J. Mechanism of Cellular Accumulation of an Iridium(Iii) Pentamethylcyclopentadienyl Anticancer Complex Containing a C,N-Chelating Ligand†. *Metallomics* **2014**, *6* (3), 682–690. https://doi.org/10.1039/c3mt00341h.

(9) Wu, J. The Enhanced Permeability and Retention (EPR) Effect: The Significance of the Concept and Methods to Enhance Its Application. *J. Pers. Med.* **2021**, *11* (8), 771. https://doi.org/10.3390/jpm11080771.

(10) Nakamura, Y.; Mochida, A.; Choyke, P. L.; Kobayashi, H. Nano-Drug Delivery: Is the Enhanced Permeability and Retention (EPR) Effect Sufficient for Curing Cancer? *Bioconjug. Chem.* **2016**, *27* (10), 2225–2238. https://doi.org/10.1021/acs.bioconjchem.6b00437.

(11) Kobayashi, H.; Turkbey, B.; Watanabe, R.; Choyke, P. L. Cancer Drug Delivery: Considerations in the Rational Design of Nanosized Bioconjugates. *Bioconjug. Chem.* **2014**, *25* (12), 2093–2100. https://doi.org/10.1021/bc500481x.

(12) Nel, A.; Ruoslahti, E.; Meng, H. New Insights into "Permeability" as in the Enhanced Permeability and Retention Effect of Cancer Nanotherapeutics. *ACS Nano* **2017**, *11* (10), 9567–9569. https://doi.org/10.1021/acsnano.7b07214.

(13) Matsumura, Y.; Maeda, H. A New Concept for Macromolecular Therapeutics in Cancer Chemotherapy: Mechanism of Tumoritropic Accumulation of Proteins and the Antitumor Agent Smancs. *Cancer Res.* **1986**, *46* (12 Pt 1), 6387–6392.

(14) Estalayo-Adrián, S.; McManus, G. J.; Dalton, H. L.; Savyasachi, A. J.; Kelly, J. M.; Gunnlaugsson, T. Functionalisation of Gold Nanoparticles with Ruthenium(II) Polypyridyl Complexes for Their Application in Cellular Imaging. *Dalton Trans.* **2020**, *49* (40), 14158–14168. https://doi.org/10.1039/D0DT02754E.

(15) Deng, Z.; Yu, L.; Cao, W.; Zheng, W.; Chen, T. A Selenium-Containing Ruthenium Complex as a Cancer Radiosensitizer, Rational Design and the Important Role of ROS-Mediated Signalling. *Chem. Commun.* **2015**, *51* (13), 2637–2640. https://doi.org/10.1039/C4CC07926D.

(16) Menon, S.; Ks, S. D.; R, S.; S, R.; S, V. K. Selenium Nanoparticles: A Potent Chemotherapeutic Agent and an Elucidation of Its Mechanism. *Colloids Surf. B Biointerfaces* **2018**, *170*, 280–292. https://doi.org/10.1016/j.colsurfb.2018.06.006.
(17) He, L.; Huang, Y.; Zhu, H.; Pang, G.; Zheng, W.; Wong, Y.-S.; Chen, T. Cancer-Targeted Monodisperse Mesoporous Silica Nanoparticles as Carrier of Ruthenium Polypyridyl Complexes to Enhance Theranostic Effects. *Adv. Funct. Mater.* **2022**, *32* (45), 2209271. https://doi.org/10.1002/adfm.202209271.
(18) Yang, D.; Guan, S.; Niu, Y.; Xie, Z.; Zhou, S.; Qu, X. Construction of a Hypoxia Responsive Upconversion Nanosensor for Tumor Imaging by Fluorescence Resonance Energy Transfer from Carbon Dots to Ruthenium Complex. *J. Mater. Chem. B* **2018**, *6* (15), 2315–2322. https://doi.org/10.1039/C8TB00278A.
(19) Maroto-Díaz, M.; Elie, B. T.; Gómez-Sal, P.; Pérez-Serrano, J.; Gómez, R.; Contel, M.; Javier de la Mata, F. Synthesis and Anticancer Activity of Carbosilane Metallodendrimers Based on Arene Ruthenium(II) Complexes. *Dalton Trans.* **2016**, *45* (16), 7049–7066. https://doi.org/10.1039/C6DT00465B.
(20) Michlewska, S.; Maroto, M.; Hołota, M.; Kubczak, M.; Sanz del Olmo, N.; Ortega, P.; Shcharbin, D.; de la Mata, F. J.; Bryszewska, M.; Ionov, M. Combined Therapy of Ruthenium Dendrimers and Anti-Cancer Drugs against Human Leukemic Cells. *Dalton Trans.* **2021**, *50* (27), 9500–9511. https://doi.org/10.1039/D1DT01388B.
(21) Michlewska, S.; Ionov, M.; Szwed, A.; Rogalska, A.; Sanz del Olmo, N.; Ortega, P.; Denel, M.; Jacenik, D.; Shcharbin, D.; de la Mata, F. J.; Bryszewska, M. Ruthenium Dendrimers against Human Lymphoblastic Leukemia 1301 Cells. *Int. J. Mol. Sci.* **2020**, *21* (11), 4119. https://doi.org/10.3390/ijms21114119.
(22) Maroto-Diaz, M.; Sanz del Olmo, N.; Muñoz-Moreno, L.; Bajo, A. M.; Carmena, M. J.; Gómez, R.; García-Gallego, S.; de la Mata, F. J. In Vitro and in Vivo Evaluation of First-Generation Carbosilane Arene Ru(II)-Metallodendrimers in Advanced Prostate Cancer. *Eur. Polym. J.* **2019**, *113*, 229–235. https://doi.org/10.1016/j.eurpolymj.2019.01.047.
(23) Gouveia, M.; Figueira, J.; Jardim, M.; Castro, R.; Tomás, H.; Rissanen, K.; Rodrigues, J. Poly(Alkylidenimine) Dendrimers Functionalized with the Organometallic Moiety [Ru(H5-C5H5)(PPh3)2]+ as Promising Drugs Against Cisplatin-Resistant Cancer Cells and Human Mesenchymal Stem Cells. *Molecules* **2018**, *23* (6), 1471. https://doi.org/10.3390/molecules23061471.
(24) Rodrigues, J.; Jardim, M. G.; Figueira, J.; Gouveia, M.; Tomás, H.; Rissanen, K. Poly(Alkylidenamines) Dendrimers as Scaffolds for the Preparation of Low-Generation Ruthenium Based Metallodendrimers. *New J. Chem.* **2011**, *35* (10), 1938–1943. https://doi.org/10.1039/C1NJ20364A.
(25) Govender, P.; Riedel, T.; Dyson, P. J.; Smith, G. S. Higher Generation Cationic N,N-Ruthenium(II)-Ethylene-Glycol-Derived Metallodendrimers: Synthesis, Characterization and Cytotoxicity. *J. Organomet. Chem.* **2015**, *799–800*, 38–44. https://doi.org/10.1016/j.jorganchem.2015.09.003.
(26) Govender, P.; Renfrew, A. K.; Clavel, C. M.; Dyson, P. J.; Therrien, B.; Smith, G. S. Antiproliferative Activity of Chelating N,O- and N,N-Ruthenium(II) Arene Functionalised Poly(Propyleneimine) Dendrimer Scaffolds. *Dalton Trans.* **2011**, *40* (5), 1158–1167. https://doi.org/10.1039/C0DT00761G.
(27) Govender, P.; Antonels, N. C.; Mattsson, J.; Renfrew, A. K.; Dyson, P. J.; Moss, J. R.; Therrien, B.; Smith, G. S. Anticancer Activity of Multinuclear Arene Ruthenium Complexes Coordinated to Dendritic Polypyridyl Scaffolds. *J. Organomet. Chem.* **2009**, *694* (21), 3470–3476. https://doi.org/10.1016/j.jorganchem.2009.06.028.

(28) Novokmet, S.; Stojic, I.; Radonjic, K.; Savic, M.; Jeremic, J. Toxic Effects of Metallopharmaceuticals. *Exp. Appl. Biomed. Res. EABR* **2017**, *18* (3), 191–194. https://doi.org/10.1515/sjecr-2016-0082.
(29) Apartsin, E.; Caminade, A. Supramolecular Self-Associations of Amphiphilic Dendrons and Their Properties. *Chem. – Eur. J.* **2021**, *27* (72), 17976–17998. https://doi.org/10.1002/chem.202102589.
(30) Neranon, K.; Alberch, L.; Ramström, O. Design, Synthesis and Self-Assembly of Functional Amphiphilic Metallodendrimers. *ChemistryOpen* **2020**, *9* (1), 45–52. https://doi.org/10.1002/open.201900298.
(31) Libera, M.; Formanek, P.; Schellkopf, L.; Trzebicka, B.; Dworak, A.; Stamm, M. Amphiphilic Dendritic Copolymers of Tert-Butyl-Glycidylether and Glycidol as a Nanocontainer for an Anticancer Ruthenium Complex. *J. Polym. Sci. Part Polym. Chem.* **2014**, *52*, 3488–3497. https://doi.org/10.1002/pola.27413.
(32) Raju, L.; Nikkhah, S. J.; Vandichel, M.; Rajkumar, E. Peripherally "Tertiary Butyl Ester" Functionalized Bipyridine Cored Dendrons: From Synthesis and Characterization to Molecular Dynamic Simulation Study. *New J. Chem.* **2023**, *47* (18), 8913–8924. https://doi.org/10.1039/D3NJ00335C.
(33) Chis, A. A.; Dobrea, C.; Morgovan, C.; Arseniu, A. M.; Rus, L. L.; Butuca, A.; Juncan, A. M.; Totan, M.; Vonica-Tincu, A. L.; Cormos, G.; Muntean, A. C.; Muresan, M. L.; Gligor, F. G.; Frum, A. Applications and Limitations of Dendrimers in Biomedicine. *Molecules* **2020**, *25* (17), 3982. https://doi.org/10.3390/molecules25173982.
(34) Wolinsky, J. B.; Grinstaff, M. W. Therapeutic and Diagnostic Applications of Dendrimers for Cancer Treatment. *Adv. Drug Deliv. Rev.* **2008**, *60* (9), 1037–1055. https://doi.org/10.1016/j.addr.2008.02.012.
(35) Lyu, Z.; Ding, L.; Huang, A. Y.-T.; Kao, C.-L.; Peng, L. Poly(Amidoamine) Dendrimers: Covalent and Supramolecular Synthesis. *Mater. Today Chem.* **2019**, *13*, 34–48. https://doi.org/10.1016/j.mtchem.2019.04.004.
(36) Labieniec-Watala, M.; Watala, C. PAMAM Dendrimers: Destined for Success or Doomed to Fail? Plain and Modified PAMAM Dendrimers in the Context of Biomedical Applications. *J. Pharm. Sci.* **2015**, *104* (1), 2–14. https://doi.org/10.1002/jps.24222.
(37) Jiwpanich, S.; Sandanaraj, B. S.; Thayumanavan, S. Fluorophore-Cored Dendrimers for Patterns in Metalloprotein Sensing. *Chem. Commun.* **2009**, No. 7, 806. https://doi.org/10.1039/b815263b.
(38) Adronov, A.; Gilat, S. L.; Fréchet, J. M. J.; Ohta, K.; Neuwahl, F. V. R.; Fleming, G. R. Light Harvesting and Energy Transfer in Laser−Dye-Labeled Poly(Aryl Ether) Dendrimers. *J. Am. Chem. Soc.* **2000**, *122* (6), 1175–1185. https://doi.org/10.1021/ja993272e.
(39) Chen, J.; Li, S.; Zhang, L.; Liu, B.; Han, Y.; Yang, G.; Li, Y. Light-Harvesting and Photoisomerization in Benzophenone and Norbornadiene-Labeled Poly(Aryl Ether) Dendrimers via Intramolecular Triplet Energy Transfer. *J. Am. Chem. Soc.* **2005**, *127* (7), 2165–2171. https://doi.org/10.1021/ja044800b.
(40) Zhang, X.; Zeng, Y.; Yu, T.; Chen, J.; Yang, G.; Li, Y. Advances in Photofunctional Dendrimers for Solar Energy Conversion. *J. Phys. Chem. Lett.* **2014**, *5* (13), 2340–2350. https://doi.org/10.1021/jz5007862.
(41) Kim, S.; Park, S. Y.; Yoshida, I.; Kawai, H.; Nagamura, T. Amplified Spontaneous Emission from the Film of Poly(Aryl Ether) Dendrimer Encapsulating Excited-State Intramolecular Proton Transfer Dye. *J. Phys. Chem. B* **2002**, *106* (36), 9291–9294. https://doi.org/10.1021/jp021048x.

(42) Lakshmi, N. V.; Mandal, D.; Ghosh, S.; Prasad, E. Multi-Stimuli-Responsive Organometallic Gels Based on Ferrocene-Linked Poly(Aryl Ether) Dendrons: Reversible Redox Switching and Pb2+-Ion Sensing. *Chem. – Eur. J.* **2014**, *20* (29), 9002–9011. https://doi.org/10.1002/chem.201400241.
(43) Juárez-Pérez, E. J.; Viñas, C.; Teixidor, F.; Santillan, R.; Farfán, N.; Abreu, A.; Yépez, R.; Núñez, R. Polyanionic Aryl Ether Metallodendrimers Based on Cobaltabisdicarbollide Derivatives. Photoluminescent Properties. *Macromolecules* **2010**, *43* (1), 150–159. https://doi.org/10.1021/ma9019575.
(44) Kannan, R.; Prabakaran, P.; Basu, R.; Pindi, C.; Senapati, S.; Muthuvijayan, V.; Prasad, E. Mechanistic Study on the Antibacterial Activity of Self-Assembled Poly(Aryl Ether)-Based Amphiphilic Dendrimers. *ACS Appl. Bio Mater.* **2019**, *2* (8), 3212–3224. https://doi.org/10.1021/acsabm.9b00140.
(45) Kannan, R.; Muthuvijayan, V.; Prasad, E. In Vitro Study of a Glucose Attached Poly(Aryl Ether) Dendron Based Gel as a Drug Carrier for a Local Anaesthetic. *New J. Chem.* **2017**, *41* (15), 7453–7462. https://doi.org/10.1039/C7NJ01420A.
(46) Sarkar, B.; Das, K.; Jyoti Ghosh, A.; Islam, R.; Saha, T.; Prasad, E.; Gardas, R. L. Poly(Alkyl Ether) Based Ionic Liquid–γ-Cyclodextrin Based Inclusion Complex and Antibacterial Activity of the Inclusion Complex. *J. Mol. Liq.* **2022**, *361*, 119571. https://doi.org/10.1016/j.molliq.2022.119571.
(47) Liko, F.; Hindré, F.; Fernandez-Megia, E. Dendrimers as Innovative Radiopharmaceuticals in Cancer Radionanotherapy. *Biomacromolecules* **2016**, *17* (10), 3103–3114. https://doi.org/10.1021/acs.biomac.6b00929.
(48) Jiwpanich, S.; Sandanaraj, B. S.; Thayumanavan, S. Fluorophore-Cored Dendrimers for Patterns in Metalloprotein Sensing. *Chem. Commun.* **2009**, No. 7, 806–808. https://doi.org/10.1039/B815263B.
(49) Lay, P. A.; Sargeson, A. M.; Taube, H.; Chou, M. H.; Creutz, C. Cis-Bis(2,2′-Bipyridine-N,N′) Complexes of Ruthenium(III)/(II) and Osmium(III)/(II). In *Inorganic Syntheses*; John Wiley & Sons, Ltd, 1986; pp 291–299. https://doi.org/10.1002/9780470132555.ch78.
(50) Thompson, A. P.; Aktulga, H. M.; Berger, R.; Bolintineanu, D. S.; Brown, W. M.; Crozier, P. S.; in 't Veld, P. J.; Kohlmeyer, A.; Moore, S. G.; Nguyen, T. D.; Shan, R.; Stevens, M. J.; Tranchida, J.; Trott, C.; Plimpton, S. J. LAMMPS - a Flexible Simulation Tool for Particle-Based Materials Modeling at the Atomic, Meso, and Continuum Scales. *Comput. Phys. Commun.* **2022**, *271*, 108171. https://doi.org/10.1016/j.cpc.2021.108171.
(51) Humphrey, W.; Dalke, A.; Schulten, K. VMD: Visual Molecular Dynamics. *J. Mol. Graph.* **1996**, *14* (1), 33–38. https://doi.org/10.1016/0263-7855(96)00018-5.
(52) Wells, B. A.; Chaffee, A. L. Ewald Summation for Molecular Simulations. *J. Chem. Theory Comput.* **2015**, *11* (8), 3684–3695. https://doi.org/10.1021/acs.jctc.5b00093.
(53) Kowsalya, E.; MosaChristas, K.; Jaquline, C. R. I.; Balashanmugam, P.; Devasena, T. Gold Nanoparticles Induced Apoptosis via Oxidative Stress and Mitochondrial Dysfunctions in MCF-7 Breast Cancer Cells. *Appl. Organomet. Chem.* **2021**, *35* (1), e6071. https://doi.org/10.1002/aoc.6071.
(54) Arunachalam, A.; Rengan, R.; Umapathy, D.; Arockiam, A. J. V. Impact of Biphenyl Benzhydrazone-Incorporated Arene Ru(II) Complexes on Cytotoxicity and the Cancer Cell Death Mechanism. *Organometallics* **2022**, *41* (17), 2474–2486. https://doi.org/10.1021/acs.organomet.2c00290.
(55) Fréchet, J. M. J.; Ihre, H.; Davey, M. Preparation of 'Fréchet-Type' Polyether Dendrons and Aliphatic Polyester Dendrimers by Convergent Growth: An Experimental Primer.

In *Dendrimers and Other Dendritic Polymers*; John Wiley & Sons, Ltd, 2001; pp 567–586. https://doi.org/10.1002/0470845821.ch24.
(56) Vögtle, F.; Plevoets, M.; Nieger, M.; Azzellini, G. C.; Credi, A.; De Cola, L.; De Marchis, V.; Venturi, M.; Balzani, V. Dendrimers with a Photoactive and Redox-Active [Ru(Bpy)3]2+-Type Core: Photophysical Properties, Electrochemical Behavior, and Excited-State Electron-Transfer Reactions. *J. Am. Chem. Soc.* **1999**, *121* (26), 6290–6298. https://doi.org/10.1021/ja990430t.
(57) Hahn, U.; Luelf, H.; Winkler, H. D. F.; Schalley, C. A.; Vögtle, F.; De Cola, L. Encapsulation of Luminescent Homoleptic [Ru(Dpp) $_3$] $^{2+}$ -Type Chromophores within an Amphiphilic Dendritic Environment. *Chem. - Eur. J.* **2012**, *18* (48), 15424–15432. https://doi.org/10.1002/chem.201201126.
(58) Baytekin, B.; Baytekin, H. T.; Hahn, U.; Reckien, W.; Kirchner, B.; Schalley, C. A. Dendrimer Disassembly in the Gas Phase: A Cascade Fragmentation Reaction of Fréchet Dendrons. *Chem. - Eur. J.* **2009**, *15* (29), 7139–7149. https://doi.org/10.1002/chem.200900403.
(59) Douloudi, M.; Nikoli, E.; Katsika, T.; Vardavoulias, M.; Arkas, M. Dendritic Polymers as Promising Additives for the Manufacturing of Hybrid Organoceramic Nanocomposites with Ameliorated Properties Suitable for an Extensive Diversity of Applications. *Nanomaterials* **2020**, *11* (1), 19. https://doi.org/10.3390/nano11010019.
(60) Prabaharan, R.; Rengan, R.; Umapathy, D.; Arockiam, A. J. V.; Małecki, J. G. Assessment of Antiproliferative Activity of New Half-sandwich Arene Ru (II) Furylbenzhydrazone Complexes. *Appl. Organomet. Chem.* **2022**, *36* (2), e6512. https://doi.org/10.1002/aoc.6512.
(61) Kamatchi, T. S.; Subarkhan, M. K. M.; Ramesh, R.; Wang, H.; Małecki, J. G. Investigation into Antiproliferative Activity and Apoptosis Mechanism of New Arene Ru(II) Carbazole-Based Hydrazone Complexes. *Dalton Trans.* **2020**, *49* (32), 11385–11395. https://doi.org/10.1039/D0DT01476A.
(62) Albertazzi, L.; Serresi, M.; Albanese, A.; Beltram, F. Dendrimer Internalization and Intracellular Trafficking in Living Cells. *Mol. Pharm.* **2010**, *7* (3), 680–688. https://doi.org/10.1021/mp9002464.
(63) Mascheroni, L.; Francia, V.; Rossotti, B.; Ranucci, E.; Ferruti, P.; Maggioni, D.; Salvati, A. Light-Triggered Trafficking to the Cell Nucleus of a Cationic Polyamidoamine Functionalized with Ruthenium Complexes. *ACS Appl. Mater. Interfaces* **2020**, *12* (31), 34576–34587. https://doi.org/10.1021/acsami.0c08033.
(64) Subarkhan, M. K. M.; Ramesh, R. Ruthenium(II) Arene Complexes Containing Benzhydrazone Ligands: Synthesis, Structure and Antiproliferative Activity. *Inorg. Chem. Front.* **2016**, *3* (10), 1245–1255. https://doi.org/10.1039/C6QI00197A.
(65) Rieger, A. M.; Nelson, K. L.; Konowalchuk, J. D.; Barreda, D. R. Modified Annexin V/Propidium Iodide Apoptosis Assay for Accurate Assessment of Cell Death. *J. Vis. Exp. JoVE* **2011**, No. 50, 2597. https://doi.org/10.3791/2597.
(66) Baecker, D.; Kapp, T.; Schumacher, P.; Gust, R.; Kircher, B. Cell Death-Inducing Properties of Selected Dendrimers against Different Breast Cancer and Leukemia Cell Lines. *Arch. Pharm. (Weinheim)* **2020**, *353* (11), e2000209. https://doi.org/10.1002/ardp.202000209.
(67) Sahu, G.; Patra, S. A.; Lima, S.; Das, S.; Görls, H.; Plass, W.; Dinda, R. Ruthenium(II)-dithiocarbazates as Anticancer Agents: Synthesis, Solution Behavior, and Mitochondria-targeted Apoptotic Cell Death. *Chem. – Eur. J.* **2023**, chem.202202694. https://doi.org/10.1002/chem.202202694.
(68) Li, Y.; Wu, Q.; Yu, G.; Li, L.; Zhao, X.; Huang, X.; Mei, W. Polypyridyl Ruthenium(II) Complex-Induced Mitochondrial Membrane Potential Dissipation Activates DNA

Damage-Mediated Apoptosis to Inhibit Liver Cancer. *Eur. J. Med. Chem.* **2019**, *164*, 282–291. https://doi.org/10.1016/j.ejmech.2018.12.041.
(69) De Grandis, R. A.; Costa, A. R.; Moraes, C. A. F.; Sampaio, N. Z.; Cerqueira, I. H.; Marques, W. G.; Guedes, A. P. M.; de Araujo-Neto, J. H.; Pavan, F. R.; Demidoff, F. C.; Netto, C. D.; Batista, A. A.; Resende, F. A. Novel Ru(II)-Bipyridine/Phenanthroline-Lapachol Complexes as Potential Anti-Cancer Agents. *J. Inorg. Biochem.* **2022**, *237*, 112005. https://doi.org/10.1016/j.jinorgbio.2022.112005.
(70) Maciel, D.; Nunes, N.; Santos, F.; Fan, Y.; Li, G.; Shen, M.; Tomás, H.; Shi, X.; Rodrigues, J. New Insights into Ruthenium(II) Metallodendrimers as Anticancer Drug Nanocarriers: From Synthesis to Preclinic Behaviour. *J. Mater. Chem. B* **2022**, *10* (43), 8945–8959. https://doi.org/10.1039/D2TB01280D.
(71) Gu, Y.-Q.; Shen, W.-Y.; Yang, Q.-Y.; Chen, Z.-F.; Liang, H. Ru(III) Complexes with Pyrazolopyrimidines as Anticancer Agents: Bioactivities and the Underlying Mechanisms. *Dalton Trans.* **2022**, *51* (4), 1333–1343. https://doi.org/10.1039/D1DT02765D.
(72) Deng, Z.; Gao, P.; Yu, L.; Ma, B.; You, Y.; Chan, L.; Mei, C.; Chen, T. Ruthenium Complexes with Phenylterpyridine Derivatives Target Cell Membrane and Trigger Death Receptors-Mediated Apoptosis in Cancer Cells. *Biomaterials* **2017**, *129*, 111–126. https://doi.org/10.1016/j.biomaterials.2017.03.017.
(73) Balaji, S.; Mohamed Subarkhan, M. K.; Ramesh, R.; Wang, H.; Semeril, D. Synthesis and Structure of Arene Ru(II) NΛO-Chelating Complexes: In Vitro Cytotoxicity and Cancer Cell Death Mechanism. *Organometallics* **2020**, *39* (8), 1366–1375. https://doi.org/10.1021/acs.organomet.0c00092.
(74) Liu, J.; Lai, H.; Xiong, Z.; Chen, B.; Chen, T. Functionalization and Cancer-Targeting Design of Ruthenium Complexes for Precise Cancer Therapy. *Chem. Commun.* **2019**, *55* (67), 9904–9914. https://doi.org/10.1039/C9CC04098F.
(75) Jiang, G.-B.; Zheng, X.; Yao, J.-H.; Han, B.-J.; Li, W.; Wang, J.; Huang, H.-L.; Liu, Y.-J. Ruthenium(II) Polypyridyl Complexes Induce BEL-7402 Cell Apoptosis by ROS-Mediated Mitochondrial Pathway. *J. Inorg. Biochem.* **2014**, *141*, 170–179. https://doi.org/10.1016/j.jinorgbio.2014.09.001.
(76) Jiang, G.-B.; Zhang, W.-Y.; He, M.; Gu, Y.-Y.; Bai, L.; Wang, Y.-J.; Yi, Q.-Y.; Du, F. Development of Four Ruthenium Polypyridyl Complexes as Antitumor Agents: Design, Biological Evaluation and Mechanism Investigation. *J. Inorg. Biochem.* **2020**, *208*, 111104. https://doi.org/10.1016/j.jinorgbio.2020.111104.
(77) Elgar, C. E.; Yusoh, N. A.; Tiley, P. R.; Kolozsvári, N.; Bennett, L. G.; Gamble, A.; Péan, E. V.; Davies, M. L.; Staples, C. J.; Ahmad, H.; Gill, M. R. Ruthenium(II) Polypyridyl Complexes as FRET Donors: Structure- and Sequence-Selective DNA-Binding and Anticancer Properties. *J. Am. Chem. Soc.* **2023**, *145* (2), 1236–1246. https://doi.org/10.1021/jacs.2c11111.
(78) Vaidyanathan, V. G.; Nair, B. U. Synthesis, Characterization and DNA Binding Studies of a Ruthenium(II) Complex. *J. Inorg. Biochem.* **2002**, *91* (2), 405–412. https://doi.org/10.1016/S0162-0134(02)00448-8.
(79) Brabec, V.; Kasparkova, J. Ruthenium Coordination Compounds of Biological and Biomedical Significance. DNA Binding Agents. *Coord. Chem. Rev.* **2018**, *376*, 75–94. https://doi.org/10.1016/j.ccr.2018.07.012.
(80) Mandal, S.; Tarai, S. K.; Patra, P.; Nandi, P.; Sing, S.; Rajak, B.; Moi, S. C. Brief Research on the Biophysical Study and Anticancer Behavior of Pt(II) Complexes: Their DNA/BSA Binding, Molecular Docking, and Cytotoxic Property. *Langmuir* **2022**, *38* (44), 13613–13625. https://doi.org/10.1021/acs.langmuir.2c02490.